ERDC TR-24-3

U.S. ARMY
US Army Corps of Engineers®
ERDC

Rapid Airfield Damage Recovery and Coalition Warfare Programs

Extreme Cold Weather Airfield Damage Repair Testing at Goose Bay Air Base, Canada

William D. Carruth, Terry D. Melendy, Jr., George L. Blaisdell, Benjamin E. Watts, Danielle Kennedy, Jeb S. Tingle, and Alessandra Bianchini

January 2024

Engineer Research and Development Center

The US Army Engineer Research and Development Center (ERDC) solves the nation's toughest engineering and environmental challenges. ERDC develops innovative solutions in civil and military engineering, geospatial sciences, water resources, and environmental sciences for the Army, the Department of Defense, civilian agencies, and our nation's public good. Find out more at www.erdc.usace.army.mil.

To search for other technical reports published by ERDC, visit the ERDC online library at https://erdclibrary.on.worldcat.org/discovery.

ERDC TR-24-3
January 2024

Extreme Cold Weather Airfield Damage Repair Testing at Goose Bay Air Base, Canada

William D. Carruth and Jeb S. Tingle

Geotechnical and Structures Laboratory (GSL)
US Army Engineer Research and Development Center (ERDC)
3909 Halls Ferry Road
Vicksburg, MS 39180-6199

Terry D. Melendy, Jr., George L. Blaisdell, Benjamin E. Watts, and Danielle Kennedy

Cold Regions Research and Engineering Laboratory (CRREL)
US Army Engineer Research and Development Center
72 Lyme Road
Hanover, NH 03755

Alessandra Bianchini

Consultant, former Air Force Civil Engineer Center Base Resilience Subject Matter Expert
3505 Hidden Valley Road
Lynn Haven, FL 32444

Final Report

Prepared for US Air Force Civil Engineer Center (AFCEC)
139 Barnes Drive, Suite 1
Tyndall AFB, FL 32403

Office of the Under Secretary of Defense for Acquisition and Sustainment – International Cooperation
1400 Defense Pentagon
Washington, DC 20301

Under Reimbursable—MIPR: HQ0642930842, AFCEC & HQ0157 OUSD (AT&L 1400), "Rapid Airfield Damage Recovery (RADR) & Coalition Warfare Program"

Abstract

Rapid Airfield Damage Recovery (RADR) technologies have proven successful in temperate and subfreezing temperatures but have not been evaluated in extreme cold weather temperatures near 0°F. To address this capability gap, laboratory-scale and full-scale testing was conducted at these temperatures. Methods developed for moderate climates were adapted and demonstrated alongside methods that used snow harvested on-site as compacted backfill. After only a few days of training, seven experimental repairs were conducted by Canadian airmen at Goose Bay Air Base in Labrador, Canada, and load tested with a single-wheel C-17 load cart. Existing RADR technologies performed adequately despite the freezing temperatures, with the main tactic, techniques, and procedures modification being an increased cure time for the rapid-setting concrete surface material. Compacted snow-water slurry methods also performed well, demonstrating their ability to withstand over 500 passes of single-wheel C-17 traffic after sufficient freezing time.

Contents

Figures and Tables

Figures

Tables

Preface

This study was conducted for the US Air Force Civil Engineer Center (AFCEC), Reimbursable—MIPR: HQ0642930842, AFCEC & HQ0157 OUSD (AT&L 1400), under the "Rapid Airfield Damage Recovery (RADR) and Coalition Warfare Program." The work was also sponsored by the Office of the Under Secretary of Defense for Acquisition and Sustainment–International Cooperation through the Coalition Warfare Program. The technical monitor was Dr. Robert Diltz of AFCEC. The Program Manager was Mr. Jeb S. Tingle.

The work was performed by the Airfields and Pavements Branch (Ms. Anna Jordan, chief) of the Engineering Systems and Materials Division (Mr. Justin Strickler, chief), US Army Engineer Research and Development Center–Geotechnical and Structures Laboratory (ERDC-GSL). The work was also performed by the Force Projection and Sustainment Branch (Dr. Orian Welling, chief) and the Engineering Resources Branch (Dr. Melisa Nallar, chief) of the Research and Engineering Division (Dr. John Weatherly, acting chief), ERDC Cold Regions Research and Engineering Laboratory (CRREL). At the time of publication, Mr. R. Nicholas Boone was the technical director for Force Projection and Maneuver Support. The deputy director of ERDC-GSL was Mr. Charles Ertle II, and the director was Mr. Bartley P. Durst. The deputy director of ERDC-CRREL was Dr. Ivan P. Beckman, and the director was Dr. Joseph L. Corriveau.

COL Christian Patterson was the commander of ERDC, and Dr. David W. Pittman was the director.

1 Introduction

1.1 Background

1.1.1 Initiation of Modern Research Efforts

Repair of damaged airfields has been an exceedingly important issue for military organizations since the beginning of aircraft use in combat. Mann et al. (2007) summarized airfield pavement repair research conducted from the 1960s to the early 1990s, including investigations involving novel materials and methods such as rapid-setting concrete (RSC), stone and grout, and cellular concrete. Traditional methods, including full slab replacement and surfacing repairs with conventional concrete and asphalt, were also included in the literature. Overall, the authors noted that while a considerable amount of work was conducted during the period, the materials and procedures did not change dramatically. The preferred expedient method for repairing craters remained: using debris to fill the crater, followed by placement of crushed stone backfill with a foreign object debris (FOD) cover (Departments of the Army et al. 2003).

The most prominent recent research program addressing airfield damage repair (ADR) began in March 2002 after the Joint Airfield Damage Repair Working Group identified the lack of certification of existing ADR methods for C-17 aircraft as the number one repair issue requiring immediate attention. The US Air Force (USAF) Air Mobility Command funded an effort by the US Army Engineer Research and Development Center (ERDC) to evaluate existing ADR expedient repair technologies under C-17 aircraft loads. Load cart testing verified that the legacy expedient repair systems provided adequate vertical load-bearing support for current aircraft, but new anchor bolts were developed and recommended for anchoring new FOD cover mats to asphalt pavements (Gartrell 2007; 2008).

In 2005, ERDC and the C-17 Systems Group conducted flight tests on the legacy expedient repair technologies at Plant 42 in Palmdale, California. The most significant shortfall noted from the evaluation of the legacy ADR expedient repair technologies was that none of the repair technologies could support C-17 aircraft on a runway where high, horizontal braking forces caused the systems to fail. For C-17 operations only, the repairs can be performed without the protective mat surfacing or FOD cover. However, protective surfacing or FOD covers are required for operation of most other aircraft. Thus, the legacy repair technologies could not be used

on airfields subjected to both fighter and heavy cargo aircraft due to the inability of the current systems to sustain C-17 operations and the inability of fighter aircraft to operate on unsurfaced repairs.

1.1.2 Critical Runway Assessment and Repair (CRATR) Joint Capabilities Technology Demonstration (JCTD)

To address the operational limitations of legacy repair methods, the Critical Runway Assessment and Repair (CRATR) Joint Capabilities Technology Demonstration (JCTD) was initiated in 2006. The intent of the CRATR JCTD was to provide a method of rapidly assessing and repairing damage to an airfield. The JCTD's goal was to develop capabilities to return damaged runways (repairing up to 100 small craters) to full operational sortie production in fewer than 8 hr. A redesign of the legacy fiber-reinforced polyester (FRP) FOD covers was also initiated by the USAF under the ADR modernization program during this time. The CRATR JCTD included three major technology demonstrations. These demonstrations included two limited operational utility assessments (LOUAs) and one operational utility assessment (OUA). LOUA1 was conducted to evaluate materials, tactics, techniques, and procedures (TTPs) and prototype equipment for rapid automated airfield damage assessment and crater repair (Tingle et al. 2009). Following material and equipment modifications, LOUA2 took place during April 2009 (Priddy et al. 2013a) so further evaluation of materials, TTPs, and prototype equipment for crater repair could take place.

Successfully demonstrated technologies from LOUA2 were down-selected and refined for a final OUA demonstration. The OUA demonstration was conducted at Avon Park Air Force Range, Florida, during August 2009 (Priddy et al. 2011a; Priddy et al. 2011b; Priddy et al. 2013b). In general, the OUA demonstration validated that the new materials, equipment, and procedures can meet the required ADR timeline and sustain live aircraft traffic. The redesigned FRP panels were also live flight certified during this time (Priddy et al. 2011b). Based on the results of the OUA, the USAF began refinement and procurement of the new crater repair technologies.

1.1.3 Further Refinement Efforts

After completion of the CRATR JCTD, numerous additional troop demonstrations and full-scale tests were conducted to address other gaps identified within the scope of what is currently referred to as the Rapid

Airfield Damage Recovery (RADR) modernization program. These include conducting repairs in cold weather (Edwards et al. 2013; 2018) and wet weather (Bell et. al 2013; Bell 2017; Bell et al. 2018) along with execution of large crater repairs (Carruth et al. 2015). Additional research was performed on equipment refinement (Bell et al. 2015; Bell and Rowland 2017), and evaluations of the structural performance of RSC (Priddy et al. 2016) and rapid-setting flowable fill (RSFF) (Carruth and Howard 2016) was conducted. Investigation and development of alternative backfill materials such as polyurethane foam (Mejias-Santiago et al. 2016; 2017), stabilized soil (Johnson et al. 2018), and geocells have also occurred.

A description of the crater repair process developed during the CRATR JCTD and further refined during the RADR modernization program is well documented in many of the references cited above (Bell et al. 2013; Priddy et al. 2013b; Edwards et al. 2013; and Carruth et al. 2015). First, large debris is removed with track loaders and large front-end loaders. Next, the stanchion method is used (USAF 1992) to mark the extent of upheaval before a square repair area on the pavement is marked. The marked area is then saw-cut followed by breaking and removal of the existing material with wheeled excavators. Once the repair is excavated, it is backfilled, typically with RSFF or compacted crushed stone. The repair is surfaced with RSC by using the USAF Simplified Volumetric Mixer (SVM).

The basic USAF RADR unit type code (UTC) is designed to provide the capability to repair 18 small craters (8.5* ft in diameter) or two large craters (30 ft in diameter) in 8 hr. To carry out this task, the UTC includes a major repair kit consisting of nearly 50 vehicles, tools, and bulk storage of all required materials. Other kits include a spall repair kit with equipment, tools, and materials for conducting smaller-sized repairs and an inclement weather kit to enable repairs to be conducted during cold or wet weather (Bell 2017).

1.2 Previous Cold Weather Rapid Airfield Damage Recovery (RADR) Testing

To evaluate the new RADR solutions developed during the CRATR JCTD, ERDC performed a cold-weather demonstration at Malmstrom Air Force

* For a full list of the unit conversions used in this document, please refer to *US Government Publishing Office Style Manual*, 31st ed. (Washington, DC: US Government Publishing Office, 2016), 345–47, https://www.govinfo.gov/content/pkg/GPO-STYLEMANUAL-2016/pdf/GPO-STYLEMANUAL-2016.pdf.

Base (AFB), Montana, in March–April 2012 (Edwards et al. 2013). The repair methods used were dry-placed RSFF backfill with an RSC surface. The ambient temperature was approximately 25°F. Repairs were successfully conducted by members of the 819th Red Horse Squadron and withstood 1,500 passes of simulated F-15E traffic with only minor environmental distresses observed.

ERDC Geotechnical and Structures Laboratory (GSL) and ERDC Cold Regions Research and Engineering Laboratory (CRREL) also previously collaborated to evaluate additives to accelerate curing of RSFF and RSC in cold temperatures. After a series of laboratory tests (Oren et al. 2014) were conducted, full-scale testing occurred in CRREL's Frost Effects Research Facility (FERF) in June 2013 (Edwards et al. 2018). This laboratory study recommended that aluminum sulfate be used as an additive to decrease the set time for RSC in cold weather. To accelerate the curing of RSFF, heating the mix water to a temperature of at least 100°F was recommended. Full-scale testing at approximately 25°F ambient temperature revealed that RSC was able to sustain traffic after approximately 2 hr of cure time when placed over RSFF placed with the SVM. Use of aluminum sulfate was attempted as an additive for RSFF but was ineffective. Heating the mix water to approximately 90°F was the best method identified for cold weather repairs that use RSFF.

1.3 Previous Experience Using Snow-Water Slurry as a Repair Material

1.3.1 Snow Runways

In Antarctica, several runways supporting wheeled aircraft are constructed entirely of snow and ice. The largest is a recently established runway near McMurdo Station which routinely supports C-17 missions (Haehnel et al. 2019). Being founded on a deep snow field and constructed entirely of compacted snow, patching of any runway damage caused by aircraft or ground equipment operations (or natural phenomena like warm temperatures) is achieved solely by using natural snow. This has proven successful and can yield a fully cured patch within 24 to 48 hr.

1.3.2 Snow as a Patching Material

Natural snow can be used to fill a cavity in a paved runway but only under limited conditions. In this case, natural snow means no water has been added manually; the snow itself may be moist due to solar heating, warm ambient temperatures, or wetting from natural liquid precipitation. Our

experience indicates that the snow used for patching needs to be between about 25°F and 30°F for it to be used "as is" to create a successful patch.

When snow in its natural state does not contain enough moisture content to allow good compaction (and subsequent intergranular bond formation), manual wetting can add to the range of application conditions. Laboratory tests (Asenath-Smith et al. 2019) show that frozen slush can be an expedient, high-performing crater repair material. Slush, a mixture of natural snow and water, works best for cavity repair in areas where frost enters the ground and persists throughout much of a winter. This provides a cold sink around and below the crater. When air temperatures are below freezing, a crater can be quickly filled with either a prepared snow-water mixture or clean dry snow (or ice cubes or shaved ice from a local ice-skating rink), slowly flooded with cold water, and left to freeze. Frozen slush can be a backfill layer or both backfill and surface layers. A frozen slush patch can be expected to perform satisfactorily under environmental conditions with ambient and ground temperatures from less than 25°F but greater than −40°F.

Ice reinforced with cellulose can also be used as an expedient crater repair material. Like frozen slush, cellulose-reinforced slurry (water-snow mixture) should be used when conditions are less than 25°F but greater than −40°F. The advantages to using the cellulose as an additive is that uniaxial compressive tests indicate about a 20% increase in strength over frozen slush by itself (Asenath-Smith et. al 2019). This advantage can be attained with additive levels of as little as 10%.

1.4 Objective and Scope

The primary objective of the work described in this report was to evaluate both new and existing RADR repair materials in the laboratory and in full-scale testing at extremely cold ambient temperatures. Standard RADR TTPs, equipment, tools, and materials, as well as some new compacted snow and ice backfill methods, were evaluated. Any exceptions are specifically noted in the report. Although enlisted Canadian airmen were used, timing results may not be completely representative due to slight differences in team sizes, equipment, and other factors.

1.5 Approach

The objectives were achieved by first reviewing previous research conducted on RADR technologies in extremely cold temperatures (between 0°F and 25°F). RSC performance was not previously tested at temperatures below 25°F, so it was evaluated in the laboratory. Select technologies were then further investigated via a full-scale experiment.

1.6 Chapter Outline

Chapter 2 describes procedures, materials, and results from the laboratory evaluation. Chapter 3 provides details regarding the test site and the equipment and materials used during full-scale testing. Chapter 4 lists the RADR crater repair processes used for full-scale testing, and Chapter 5 provides test results and discussion. Conclusions and recommendations can be found in Chapter 6. Appendix A contains hourly weather data tables for the entire full-scale test, and Appendix B describes a detailed compacted snow and ice placement procedure.

2 Laboratory Testing

2.1 Background

The use of conventional cast concrete cylinders to measure compressive strength in a cold weather ADR setting is challenging due to differences in size, mass, and boundary conditions between test specimens and slab repairs. One study (Edwards et al. 2018) evaluated the full-scale performance of existing two-stage RADR solutions using heated curing water to compensate for lower ambient temperatures. This study identified challenges associated with the use of conventional cast cylinder specimens for estimating in-place unconfined compressive strength (UCS) due to differences in thermal mass and heat flux. The UCS of cylinder specimens cured in the same ambient temperatures as the test slab did not correlate to the level of performance obtained from the slabs during loading. The study also postulated that the properties of RADR materials vary spatially due to variations in curing temperature with the edges of a repair area showing the greatest variation. Ambient temperatures during this testing program varied from 27°F to 31°F; the materials used were conditioned in the same environment.

The issues described in the previous paragraph preclude typical concrete laboratory testing methodology for assessment of RSC materials in subfreezing temperatures on a small scale. A laboratory study was conducted to replicate the thermal environment of RSC in a typical airfield repair slab to better understand the behavior of RSC at low temperatures. This study serves as a focused investigation of methods to evaluate and ensure cold temperature performance of RSC as used in ADR. The goals were to enable use of the material in ambient temperatures as low as 15°F and to assess the impact of cold temperatures on the time required to return the repaired pavement to service. In normal temperature conditions, the RADR system enables a runway patch to be put into service with a 2 hr cure; from past research, an RSC UCS of greater than 2,500 psi is necessary to achieve this goal.

2.2 Approach

It was necessary to simulate the thermal environment of a typical airfield repair on a laboratory scale to assess the performance of RSC at low ambient temperatures. Having the ability to quickly obtain specimens for

UCS testing is important due to the short cure times that are typically important to RADR applications. Capturing previously identified geometric variations in UCS was also identified as a priority. The Concrete Airfield Repair Thermal Simulator (CARTS), a specialized apparatus, was created to meet these requirements.

2.2.1 Concrete Airfield Repair Thermal Simulator (CARTS) Design

The CARTS apparatus was created to enable cold curing and rapid testing of RSC specimens in a realistic thermal environment. To meet this objective, several design criteria were specified:

1. Be dimensionally consistent to a typical RADR repair patch.
2. Be constructed of materials which have thermal properties like a typical RADR repair patch prior to placement of RSC.
3. Allow realistic thermal conditioning of RADR patch materials.
4. Allow creation of RSC specimens at 15°F ambient temperatures.
5. Enable simultaneous curing of specimens for multiple testing ages.
6. Enable rapid testing of concrete specimens at desired testing ages.
7. Be slightly conservative in comparison to a typical RADR patch.

To address these criteria, a typical RADR patch was used as a point of reference. In general, RADR patches consist of a layer of volumetrically mixed flowable fill (VMFF) followed by a cap of RSC. The VMFF layer can range in thickness from 20 to 30 in., while the RSC layer is generally 8 to 12 in. thick. RADR patches are typically placed in conventional concrete runways, which vary in construction, but generally consist of a thick layer of concrete (12 to 16 in.) on top of a stabilized or granular base. At low ambient temperatures, the RSC in a RADR patch will be placed in an area surrounded by materials that are in thermal equilibrium with the ambient conditions. Existing runway concrete surrounding the patch will pull heat away from the curing RSC, leading to lower temperatures and potentially less strength at the edges and corners of the slab repair. A corner, having two heat transfer boundaries, generally experiences more thermal loss than an edge. This effect has been identified in past demonstrations completed in the ERDC FERF (Edwards et al. 2018) but has not been captured at a laboratory scale.

With these considerations in mind, CARTS was created to simulate the corner of a RADR patch surrounded by conventional, fully cured concrete on two sides of the simulated pavement surface and VMFF underneath.

The apparatus is pictured in Figure 1. The dimensions of CARTS were driven by the geometry of a typical RADR patch combined with a need for conservatism as well as several constraints resulting from the testing location and volume of material available.

To enable CARTS to be conditioned at an ambient temperature of 15°F, the entire apparatus was sized to fit on a conventional pallet jack. This allowed the apparatus to be constructed and stored in normal laboratory temperature conditions (approximately 73°F) and then moved into a cold room at CRREL to reach thermal equilibrium with the testing temperature. The overall area of CARTS was set at 24 in. × 24 in., with a total thickness of 16 in. During construction of CARTS, the total area was filled with VMFF to a depth of 10 in. After curing of the VMFF, the remainder of the thickness was filled with a conventional 7-sack concrete mix with a 0.42 w/c. A 12 in. × 12 in. area of the top 6 in. was left empty to create the void for a simulated patch corner. Figure 2 illustrates the dimensioned drawings of the mold used to create the CARTS apparatus.

Figure 1. Concrete Airfield Repair Thermal Simulator (CARTS) apparatus with one side of the mold removed, showing a simulated patch area, and pallet jack underneath.

Figure 2. Dimensioned drawings of the CARTS apparatus. Dimensions are in inches.

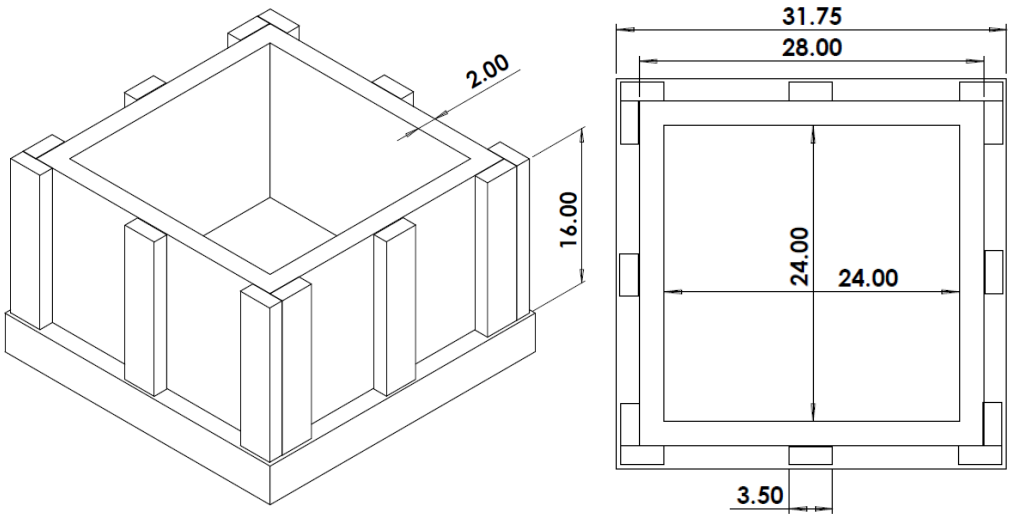

The dimensions of the simulated patch corner (12 in. × 12 in. × 6 in.) allowed nine 3 in. diameter by 6 in. tall (3 in. × 6 in.) cylinders to be obtained and tested from the curing RSC. By setting the thickness of the simulated patch corner at 6 in., well under the typical thickness of a RADR RSC cap (10 in.), the strengths obtained from the patch area should be somewhat less than those of a full thickness cap, providing some degree of conservatism. The smaller thickness also enabled multiple rounds of testing with the limited quantities of material available during the short time frame of this study.

In a typical RADR patch, the corner of the patch area would be surrounded on two sides by a large quantity of curing RSC and on the other two sides by a large quantity of existing concrete. While this is not possible to replicate exactly on a laboratory scale, the approximation of this condition can be created by heavily insulating the boundaries of the CARTS apparatus. This limits heat loss out of the curing RSC in the simulated patch area along the boundaries where more RSC would be present in a real patch. To accomplish this, the vertical boundaries of CARTS were created using 2 in. thick expanded polystyrene R-10 insulation.

CARTS was constructed to enable rapid testing of the curing RSC in a short time frame. To accomplish this, a modified procedure based on the ASTM C873 (2015) specification for cast-in-place cylinders was developed. Prior to casting, the nine 3 in. × 6 in. cylinder specimen molds used to obtain specimens were temporarily attached to a thin steel plate with hot melt adhesive. The steel plate was used to promote heat transfer to the

cured VMFF below the simulated patch corner and to prevent a mechanical bond from forming between the RSC and the VMFF. Each cylinder mold had a small hole drilled in the bottom prior to attachment to the thin steel plate. The cylinder-plate assembly was placed in the simulated patch area, and a thin plastic sheet was placed along the boundary surface between the existing concrete and the simulated patch area. As with the steel plate, this prevented a mechanical bond from forming between the RSC and the existing concrete while still enabling heat transfer. Figure 3 depicts a fully assembled CARTS apparatus in a cold room. This setup enabled rapid testing of the concrete specimens, limiting their time outside the low temperature environment of the cold room by allowing the specimen block to be removed as a unit. This also enabled convenient reuse of the CARTS apparatus.

Figure 3. Fully assembled CARTS apparatus in the cold room, ready for testing.

2.2.2 Concrete Curing

Based on past research, heated curing water was determined to be the most effective method of ensuring strength for airfield pavement patch repairs using RSC in below freezing temperatures (Oren et al. 2014; Edwards et al. 2018). These results were replicated and verified in a laboratory setting using the simulated patch area. Guidance was developed to determine the required fresh concrete temperature for successful curing at below freezing temperatures. RSC hydration is exothermic and can provide enough heat to self-cure if the rate of heat liberated through the reaction exceeds the rate of heat lost to the surroundings. Liquid water must also be available for the hydration reaction to proceed; if complete freezing of water occurs, it must occur after the chemical hydration has proceeded to the point of providing adequate compressive strength to the hardened concrete. The initial temperature of the concrete in place, the ambient temperature, and the thermal boundary conditions of the slab all play a role in determining whether enough strength will be gained prior to freezing.

2.2.3 Testing Methodology

This testing plan was established as an exploratory laboratory program to determine whether RSC could gain strength in 15°F ambient conditions and, if so, how long it would take. Previous research reported RSC provided adequate strengths with ambient temperatures of approximately 35°F (Edwards et al. 2013). Specifically, a 6 × 6 ft crater with 22 in. of VMFF and a 10 in. thick cap of RSC was able to withstand over 100 passes from a simulated F-15E aircraft after 2 hr of cure time. This laboratory study explored using the CARTS apparatus in colder temperatures to measure strength using 3 in. × 6 in. cylinders to determine, on a smaller scale, whether RSC could be a viable option in cold regions.

Five mixtures were created with the goal of determining the required fresh temperature of RSC to provide strengths in a time frame equivalent to that of a typical temperature RADR. The two primary variables for the study were target fresh temperature using heated water, and testing age. Table 1 shows the age variation, target fresh, and curing temperature. A variable that was changed for the final mix was the curing temperature. After finding success with Mix 4, researchers wanted to test with a longer initial testing age, a fresh temperature representing minimal heating of water, and a colder curing temperature.

Table 1. Target testing ages and fresh and curing temperatures for the five mixtures.

Mix Number	Testing Ages	Fresh Temperature Target	Curing Temperature
1	2 hr, 24 hr	40°F	15°F
2	2 hr, 4 hr	40°F	15°F
3	2 hr, 4 hr	50°F	15°F
4	2 hr, 4 hr	70°F	15°F
5	8 hr, 24 hr	45°F	10°F

Mixes 1 through 4 were mixed and cured in a 15°F cold room, and Mix 5 was mixed and cured in a 10°F cold room. Before mixing, the CARTS apparatus was conditioned in the cold room for at least 24 hr. Mix 1, which was based heavily on the previous research completed by Edwards et al. (2018), included testing ages of 2 and 24 hr and a fresh temperature of 40°F. Following Mix 1, the testing time frame and fresh temperature targets were adjusted for each mix to be able to reach adequate strengths in a time frame comparable to that of typical RADR testing for room temperature.

2.3 Test Procedures

2.3.1 Materials

CTS RapidSet® concrete mix was used as the tested construction material for this research due to its proven use in previous RADR demonstrations. This material was packaged in 5 gal. premixed buckets, and only water was added in the recommended quantity. All mixtures contained the same water-to-cement ratio and materials. No additional additives were incorporated into the mixture.

2.3.2 Procedures

Mixtures were designed to meet a target temperature during mixing. To accomplish this, heated tap water was used. Target temperatures ranged from 40°F to 70°F and are shown in Table 1. Water temperature was determined based on the target fresh temperature, temperature of the CTS RapidSet, an estimate of its specific heat capacity, and the final thermal mass of the mixture. The RSC was mixed for up to 5 mins until fully combined and then placed into the nine cylindrical molds and surrounding area. Specimens were made in two lifts and vibrated after each lift. Temperature was taken immediately after mixing and again after the specimens were constructed. The top surfaces of the specimens were troweled until smooth, as depicted in Figure 4. Two sets of specimens were

mixed and cast in the CARTS apparatus in the cold room for each mixture. This allowed for each mix design to be tested at two different ages.

Figure 4. Troweling surface of specimens.

All specimens were mixed and cured in below freezing temperatures. Modifications were made to testing specifications regarding testing age and curing temperatures to match test plan requirements. UCS was measured at varying ages for each mixture according to ASTM C39 (2021) using neoprene caps. Table 1 shows the testing ages for each mixture. Two test apparatuses of nine specimens each were made for each mixture to measure the strengths as specimens aged.

Specimens were demolded by removing the 12 in. × 12 in. block from the CARTS apparatus, using compressed air to blow through the base of the molds to remove the 3 in. × 6 in. cylindrical specimens (Figure 5). Specimens were numbered to document from which section of the apparatus they had been removed and were removed in order of 1 through 9, as shown in Figure 6. Two team members worked together after removing the apparatus from the cold room to quickly demold and test the specimens. Caution was taken not to warm the specimens by handling

them too often so they could be tested using unbonded neoprene caps in their cold condition.

Figure 5. Removing specimens from the mold.

Figure 6. Labeling schematic for specimens.

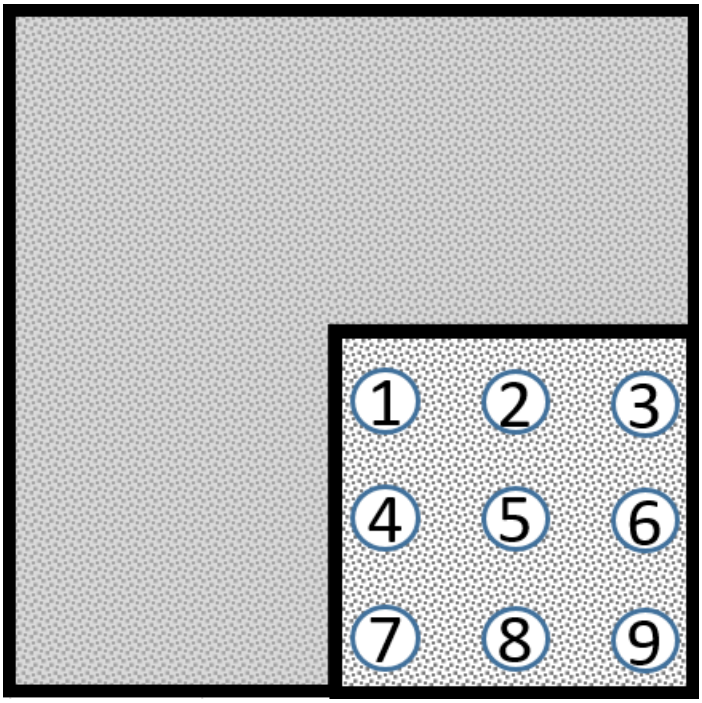

2.4 Results and Analysis

For standard compression testing, specimens are created in triplicate and strengths are determined based on the average. With the specialized apparatus, CARTS, created to mimic a RADR patch, creating multiple specimens with the same spatial characteristics was not possible. However, due to the geometry, several pairs of specimens were expected to perform similarly. Specimens were expected to react in pairs for 2 and 4, 3 and 7, and 6 and 8, based on their locations in the CARTS apparatus. Results showed that this was not always the case likely due to differences in specimen demolding and testing times that allowed the exothermic reaction to continue longer for some specimens.

Specimen 1, placed in the corner of two cold-soaked existing concrete sections, was expected to be the slowest to gain strength when compared to all other specimens. Specimen 9, which was placed on the outside corner of the apparatus and against two corners of insulation, was expected to gain strength the quickest. Specimens were tested immediately upon removal, in the order of 1 through 9, which allowed higher numbered specimens to cure longer than lower numbered specimens. Although researchers moved quickly to demold and test all specimens, this was a procedural inconsistency that likely allowed some specimens to gain more strength than others.

The first iteration of testing was based on historical work and was conducted at 15°F with a target fresh temperature of 40°F. Specimens were measured for UCS at 2 hr and 24 hr. Figure 7 shows the results of the first round of testing. The coloring scheme for the results shows a scale from red to green for lowest to highest strengths, respectively. Specimens tested at 2 hr of age generally did not exhibit significant spatial variation in UCS. However, after 24 hr of curing, the strengths exhibited spatial variation that was similar to that postulated in previous studies, with the weakest specimens occurring at the corners, followed by the those at the edges.

The weakest specimen, #1, had a strength of over 4,700 psi, while the strongest specimen, #3, achieved a strength of nearly 6,400 psi. The overall average strength at 24 hr was about 5,900 psi. After seeing low strengths after 2 hr of curing but adequate strengths at 24 hr, the second round of testing attempted to determine a shorter testing time frame than

24 hr that would produce acceptable strengths while maintaining a 15°F curing temperature.

Figure 7. Mix 1: 2 hr (*left*) and 24 hr (*right*) unconfined compressive strength (UCS) in psi.

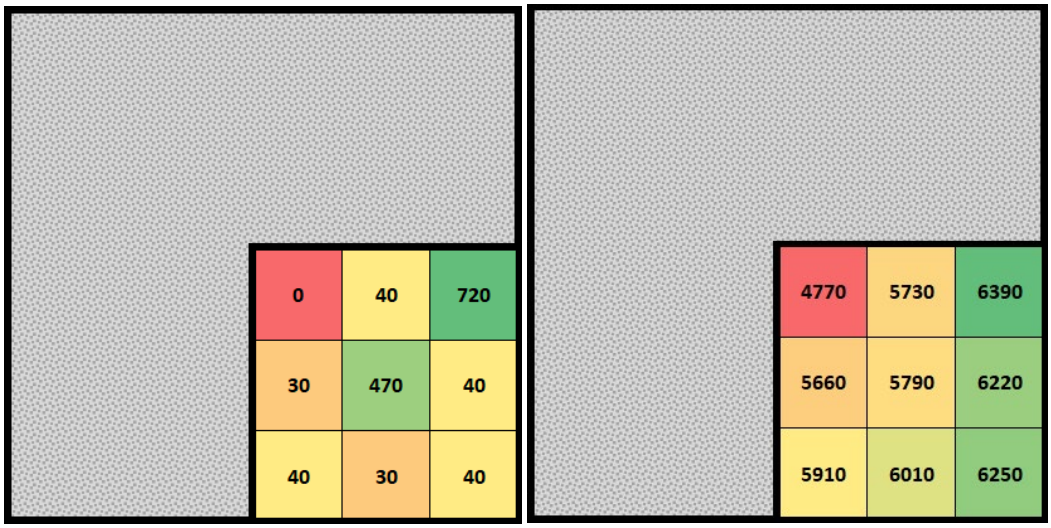

The second round of testing was completed after curing specimens at 15°F for 2 hr and 4 hr, with a target fresh temperature of 40°F. Results of this round of testing are depicted in Figure 8. Specimens removed from the cold room and tested at the age of 2 hr did not exceed 50 psi, with an overall average of approximately 35 psi. Specimens removed and tested after 4 hr also exhibited minimal strength gain with a maximum value of 780 psi and an overall average of approximately 290 psi.

Figure 8. Mix 2: 2 hr (*left*) and 4 hr (*right*) UCS in psi.

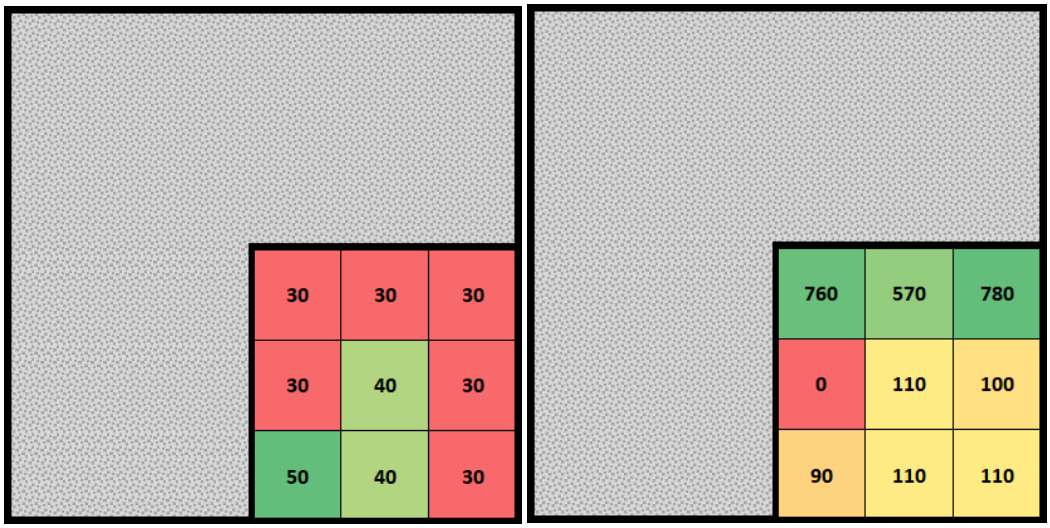

The third iteration of testing remained at 2 hr and 4 hr, but the fresh temperature target was increased to 50°F while the curing temperature remained at 15°F. On average, strengths increased for the 2 hr specimens, and there was not a major increase in strength from the 2 hr to the 4 hr curing times. Figure 9 depicts the results for the third round of testing; the average 2 hr UCS was approximately 120 psi, while the average 4 hr UCS was approximately 100 psi. This indicated that a fresh temperature of 50°F was not suitable to achieve adequate UCS at 4 hr of age.

Figure 9. Mix 3: 2 hr (*left*) and 4 hr (*right*) compressive strengths in psi.

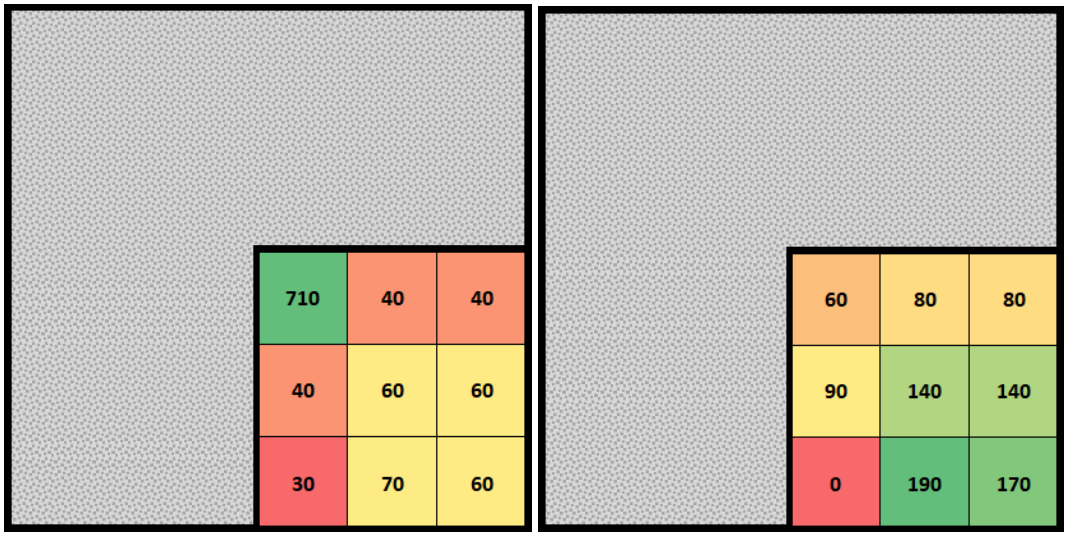

For the fourth iteration of testing, specimens were again measured at 2 hr and 4 hr and cured in a 15°F environment, but the fresh temperature target was increased to 70°F. Figure 10 provides the results from Mix 4. This iteration proved to be the most successful, with the greatest strength at 2 hr over 6,800 psi. Average UCS across all specimens at 2 hr was about 4,400 psi. The interior and exterior corner specimens (1 and 9) achieved the lowest strengths at 2 hr. However, all specimens cured for 4 hr showed strengths of at least 5,000 psi. Average UCS across the nine specimens at 4 hr was about 6,400 psi. This fourth iteration proved that an elevated fresh temperature produced significant UCS in a 15°F ambient condition in a time frame comparable to that of typical RADR. Spatial effects were observed at 2 hr of age; however, by 4 hr of curing, UCS uniformly exceeded 5,000 psi.

Figure 10. Mix 4: 2 hr (*left*) and 4 hr (*right*) UCS in psi.

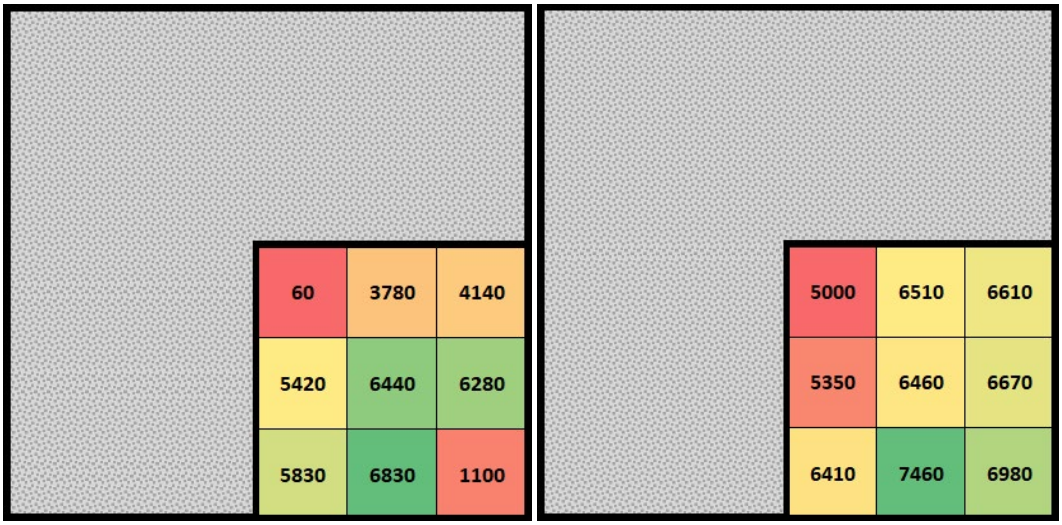

After seeing success during the fourth round of testing, the fifth and final iteration measured strengths at 8 hr and 24 hr with a target fresh temperature of 45°F and a curing temperature of 10°F. During previous testing at 40°F and 50°F, adequate strengths were seen only in specimens cured for 24 hr, with poor strengths at both 2 hr and 4 hr. Lowering the curing temperature allowed researchers to better understand the strength gain of the material at 24 hr, while also seeing whether there was strength gain at an age between the unsuccessful 4 hr and successful 24 hr ages.

Results of this final round are presented in Figure 11. Average UCS at 8 hr was approximately 3,000 psi, with a significant degree of spatial variation. The lowest UCS generally occurred at the inside corner and edges, with the highest in the center and outside corner. This is consistent with the spatial variations postulated in previous large-scale cold weather exercises. At 24 hr, the average UCS for the nine specimens was about 4,100 psi. Spatial variations were similar to the 8 hr results with higher strengths across the board. While strengths were not as high as the fourth iteration with a fresh temperature of 70°F, the results indicated that an extended curing time combined with a moderate amount of heating could produce useful UCS at a slightly colder temperature.

Figure 11. Mix 5: 8 hr (*left*) and 24 hr (*right*) UCS in psi.

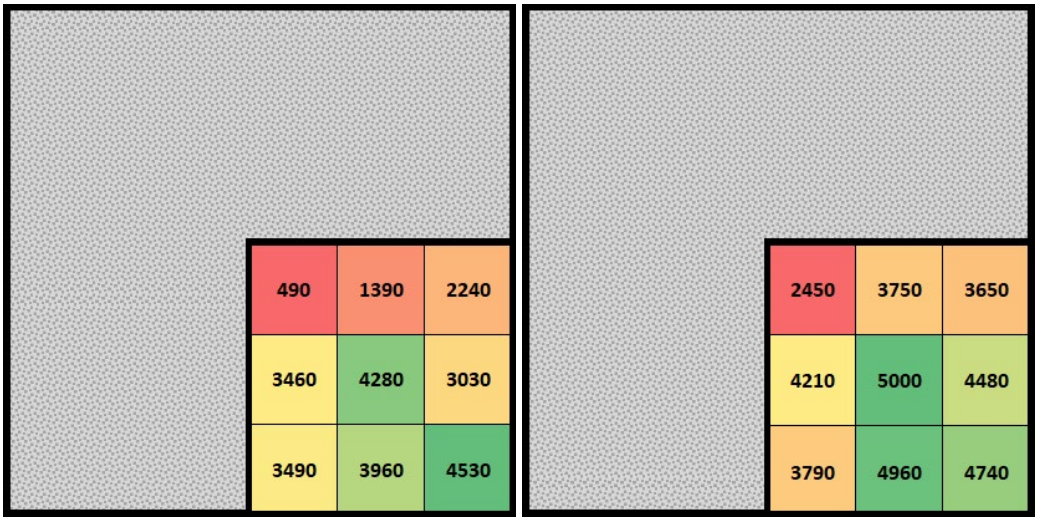

The CARTS apparatus and the method by which specimens were tested created some artifacts which are not representative of a full-scale RADR slab. The first artifact, which can be seen in the UCS numbers, has to do with both the testing time frame and the testing environment of the specimens. While the CARTS apparatus allowed all specimens to be tested in a short time frame, typically less than 30 min, the room temperature environment in which specimens were tested may have enabled sudden strength gain. This, combined with the distinct sequence in which the specimens were tested, created an obvious increase in strength in specimens tested later in the sequence. Ideally, specimen pairs with diagonal symmetry in the apparatus (2 and 4, 3 and 7, and 6 and 8) should experience the same curing conditions and have similar strengths; however, specimens later in the sequence spent more time in a room-temperature laboratory prior to testing.

The design of the mold resulted in an artifact specifically related to specimen 9, which in certain conditions did not gain strength as quickly as specimens 3, 5, or 7. This was due to the insulation boundary on the outside corner. While intended to prevent heat from leaving that surface and to simulate the presence of RSC, in reality some heat was lost through the insulation. This may have resulted in an artificially low strength in specimen 9 at early ages, which would not be expected in an actual RADR slab.

The use of heated water was successful, both in providing a minimum temperature to allow for successful curing of the RSC out to 24 hr and in accelerating the curing of RSC to match the return-to-service time of the

RADR system in normal conditions. This solution has several advantages, the most obvious of which is its simplicity. To implement heating of water in a field setting, a suitable retrofit for the SVM should be investigated. It may be possible to use off-the-shelf diesel-fired coolant heaters or on-demand water heaters in combination with existing equipment to achieve the desired result.

Overall, the UCS results from the CARTS apparatus captured the spatial trends observed in previous research, while maintaining some amount of conservatism relative to a typical RADR patch. It also allowed for useful quantification of the effects of an increase in fresh temperature on the strength development of RSC in cold ambient temperatures. The results of this study indicate that the low-temperature performance of the RSC material used for RADR patches may have more potential than previously realized and lays the groundwork for a useful path towards a more effective use of the system in arctic conditions.

2.5 Laboratory Testing Conclusions and Recommendations

This small laboratory study proved that RSC—when mixed with heated water—can be a viable option for RADR in ambient conditions down to 10°F. The following conclusions were drawn from this study:

- Adequate strengths can be expected in a cold-soaked RADR patch after 4 hr of curing with a fresh temperature of 70°F and ambient temperatures of 15°F.
- One test showed that a cold-soaked RADR patch with a fresh temperature of 45°F and ambient temperatures of 10°F would also gain sufficient strengths within 24 hr.
- The CARTS apparatus provided a conservative but realistic laboratory-scale method for testing the performance of RADR materials in different environmental conditions.

The following recommendations from this laboratory-scale study are provided:

- A larger-scale laboratory study with more iterations of fresh temperature, curing temperature, and testing times is warranted.
- The CARTS apparatus should be modified to enable demolding and testing of all specimens in a shorter time frame.

- The rebound hammer should be incorporated into the testing program to correlate strengths and provide rapid strength estimates.
- The SVM should be modified to enable heating of mix water.

3 Test Site, Equipment, and Material Descriptions

3.1 Test Site Description

Full-scale extreme cold weather ADR testing was conducted from 19–31 January 2020 on an inactive airfield apron on Goose Bay Air Base, Newfoundland and Labrador, Canada. A 1,000 ft long by 150 ft wide test area was provided, and base personnel began clearing snow in early fall 2019 to ensure the area would be clear for testing in January 2020. An existing hangar located approximately 3,000 ft from the test site was used to store equipment, materials, and tools. The hangar temperature was kept at approximately 50°F. Figure 12 shows an aerial view of the test site. Figure 13 shows the location for each repair. Note that the taxiway that enters the test site at the bottom of Figure 12 corresponds to the snow-cleared corridor in Figure 13. Crater 1 was used for a training repair first and later as a washout area for the concrete mixer, and craters 2 through 7 correspond to repairs 2 through 7 that are discussed in Chapter 5 of this report.

Figure 12. Aerial view of the test site location.

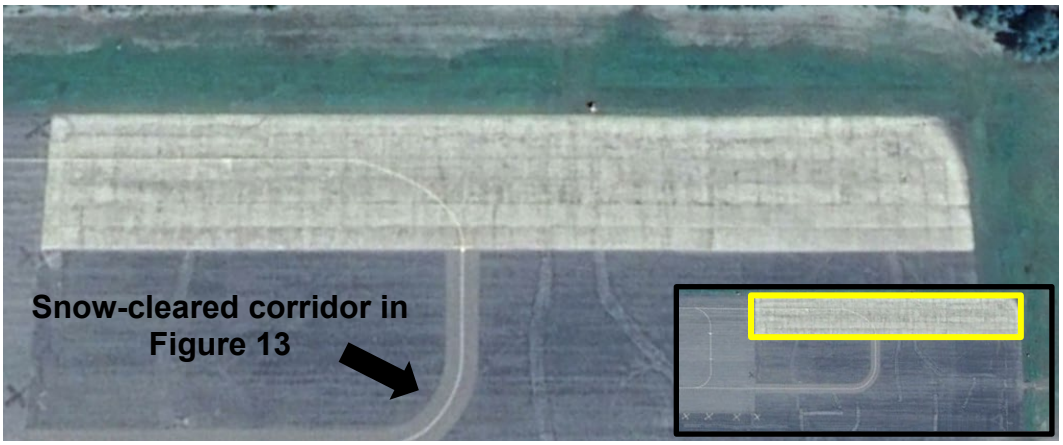

Figure 13. Crater repair locations.

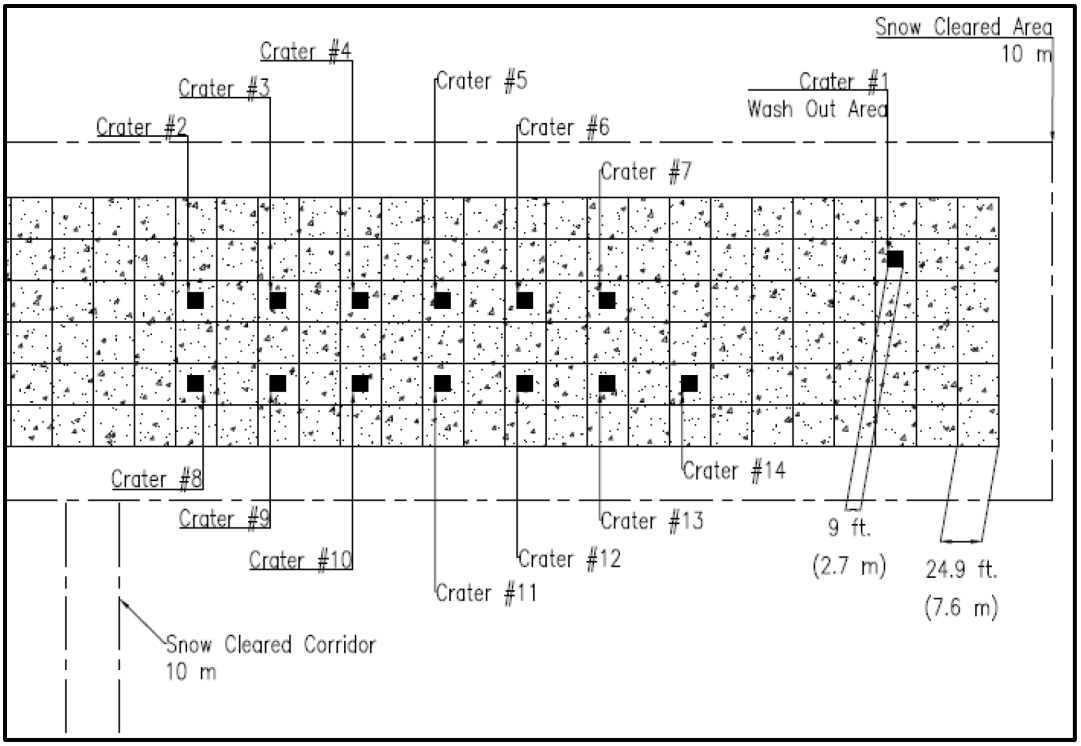

The pavement structure of the test site was approximately 13 to 14 in. of portland cement concrete (PCC) over 6 in. of stabilized sandy base material. The slab sizes were approximately 20 ft × 20 ft. The subgrade appeared to be a sandy material. Core samples of the existing PCC were extracted for UCS testing. The average UCS was 7,005 psi. The California Bearing Ratio (CBR) of the existing subgrade was estimated via dynamic cone penetrometer (DCP) testing per ASTM D6951 (2018). Figure 14 provides a representative plot of CBR versus depth. As shown, if the first 6 in. is ignored due to lack of confinement, the CBR of the first few inches of the subgrade appear to be near 10% before a stiff, likely frozen layer (70 to 100 CBR) was encountered.

Figure 14. California Bearing Ratio (CBR) versus depth plot from dynamic cone penetrometer (DCP) testing of subgrade.

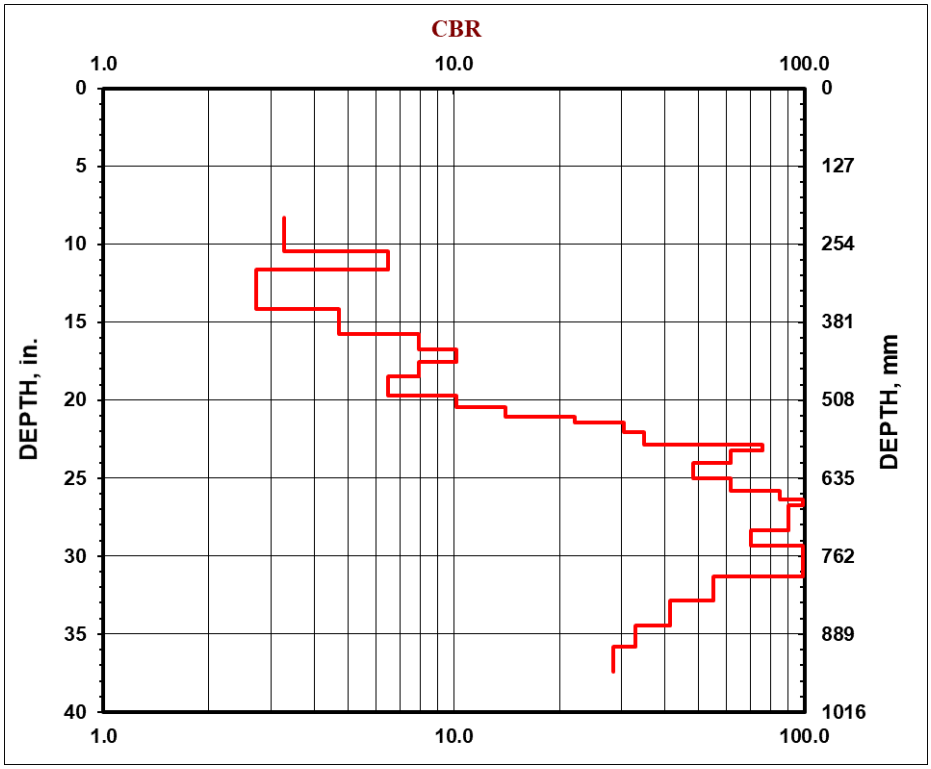

3.2 Equipment

3.2.1 Caterpillar 279D Compact Terrain Loader

Caterpillar 279D XPS and 289D XPS model compact track loaders (CTLs), or skid steers, are rubber-tracked machines with high-flow hydraulics employed for a variety of purposes in the RADR process. Figure 15 shows both models of CTLs used, and Table 2 provides the specifications. The CTLs were used for rapidly cutting around the pavement upheaval using wheel saw attachments, removing debris using bucket attachments, powering the snowblower attachment, and cleaning up using broom attachments. The machines were equipped with quick disconnect fittings that allowed the attachments to be exchanged rapidly without the use of tools.

Figure 15. Caterpillar compact track loaders (CTLs) (279D *left*, 289D *right*).

Table 2. Caterpillar CTL specifications.

Specification	Caterpillar 279D XPS	Caterpillar 289D XPS
Net Power (hp)	72.9	72.9
Operating Weight (lb)	9,893	10,533
Rated Operating Capacity at 50% Tipping Load (lb)	2,935	3,800
Travel Speed (mph)	4.5	4.5
Tipping Load (lb)	5,870	7,600
Breakout Force (lb)	7,285	7,291
Max Loader Hydraulic Pressure (psi)	4,061	4,061
Max Loader Hydraulic Flow (gal./min)	32	32
Overall Length (in.)	117.9	117.9
Height–Top of Cab (in.)	83.2	83.2
Width (in.)	78.0	78.0

3.2.1.1 Wheel Saw Attachment

The Caterpillar CTLs were equipped to operate the Caterpillar SW360B wheel saw attachment (Figure 16). The attachment provides a 3.5 in. wide cut with a maximum depth of 24 in. The wheel saw is equipped with a hydraulic side shift to assist in wheel positioning. Specifications can be

found in Table 3. Kennametal SC3-01P conical bits were primarily used on the wheel saws. Caterpillar wheel saw teeth (model number 561-8132) were used as replacements, as noted in the test results provided in Chapter 6 of this report.

Figure 16. Caterpillar 279D with SW360 wheel saw attachment.

Table 3. Wheel saw specifications.

Specification	Caterpillar SW360B
Overall Width (in.)	73
Overall Height (in.)	70
Length (in.)	93
Weight (lb)	3,420
Wheel Width (in.)	3
Required Hydraulic Flow (gpm)	33
Optimal Hydraulic Pressure (psi)	3,335
Wheel Speed at Maximum Flow (rpm)	74
Conical Bits per Wheel	70
Maximum Depth of Cut (in.)	24
Side-Shift Travel (in.)	22

3.2.1.2 Snowblower Attachment

The Caterpillar SR321 snowblower attachment (Figure 17) was used to remove clumps of snow from the stockpiles of harvested snow so the snow could be used as a crater repair backfill material. Specifications for the SR321 are provided in Table 4. The attachment uses the auger to break up clumps, and the snow is discharged through the top chute. The chute can be rotated up to 270 degrees, and the hydraulically controlled deflector dictates how far the snow is discharged.

Figure 17. Caterpillar SR321 snowblower attachment.

Table 4. Caterpillar SR321 specifications.

Specification	Value
Intake Width	76.5 in.
Overall Width	85.9 in.
Weight	1,016.3 lb
Overall Height	72.6 in.
Overall Length	37.4 in.
Required Hydraulics	High Flow XPS
Optimal Hydraulic Flow	100–125 L/min (26–33 gpm)
Optimal Hydraulic Pressure	200–280 bar (2,800–4,100 psi)
Cutting Height	34.1 in.
Maximum Throw	40 ft
Auger Diameter	18 in.
Impeller Fan Diameter	25 in.
Impeller Fan Width	8.7 in.
Chute Rotation	270 degrees

3.2.2 Excavators

Two different sized excavators were used for testing: a Caterpillar 329D (Figure 18) and a Caterpillar 308E (Figure 19). Typically, wheeled excavators are used for the RADR process. However, none were available for this experiment, so the two tracked versions were used as substitutes. Specifications for the 329D and 308E can be found in Table 5.

Figure 18. Caterpillar 329D.

Figure 19. Caterpillar 308E.

Table 5. Caterpillar 329D and 308E specifications.

Specification	Caterpillar 329D	Caterpillar 308E
Net Power (hp)	202	70.3
Maximum Digging Reach (ft)	31.0	31.0
Maximum Digging Depth (ft)	20.1	15.3
Maximum Travel Speed (mph)	3.3	3.2
Operating Weight (lb)	64,463	20,678
Overall Width (ft)	11 .1	7.6
Shipping Length (ft)	32.4	21.6
Height to Top of Cab (ft)	10.67	8.3

3.2.3 Front-end Loaders

A Caterpillar 939K front-end loader was used for general material transport, particularly for placing snow and sand during backfill operations and for clearing debris (Figure 20). The 938K uses the CAT® C7.1 with a maximum gross power of 190 hp and a maximum gross torque of 660 ft-lb. The operating weight of the 938K was 33,691 lb.

Figure 20. Caterpillar 938K front-end loader.

3.2.4 Extendable Boom Forklift

A Caterpillar TL1055D telehandler (Figure 21) was used for transporting and loading the SVM with bulk super sacks of the RSC and backfilling repairs with sand or RSFF. The super sacks of cementitious material weighed approximately 3,000 lb. Table 6 gives specifications of the Caterpillar TL1055D telehandler.

Figure 21. Caterpillar TL1055D telehandler.

Table 6. Caterpillar TL1055D telehandler specifications.

Specification	Value
Maximum Gross Power (hp)	142.1
Operating Weight (lb)	31,879
Rated Load Capacity (lb)	10,000
Maximum Lift Height (ft)	54.9
Maximum Forward Reach (ft)	42.0
Maximum Travel Speed (mph)	20.5
Length (ft)	20.7
Width (ft)	8.4
Height (ft)	8.4

3.2.5 Dump Truck

A standard dump truck with an approximate capacity of 12 cu yd was used for transporting bulk super sacks of material from the storage facility to the test site and for general hauling of debris. The hinged door was removed in some cases to ease loading of the super sacks. Figure 22 shows the dump truck used.

Figure 22. A 12 cu yd dump truck.

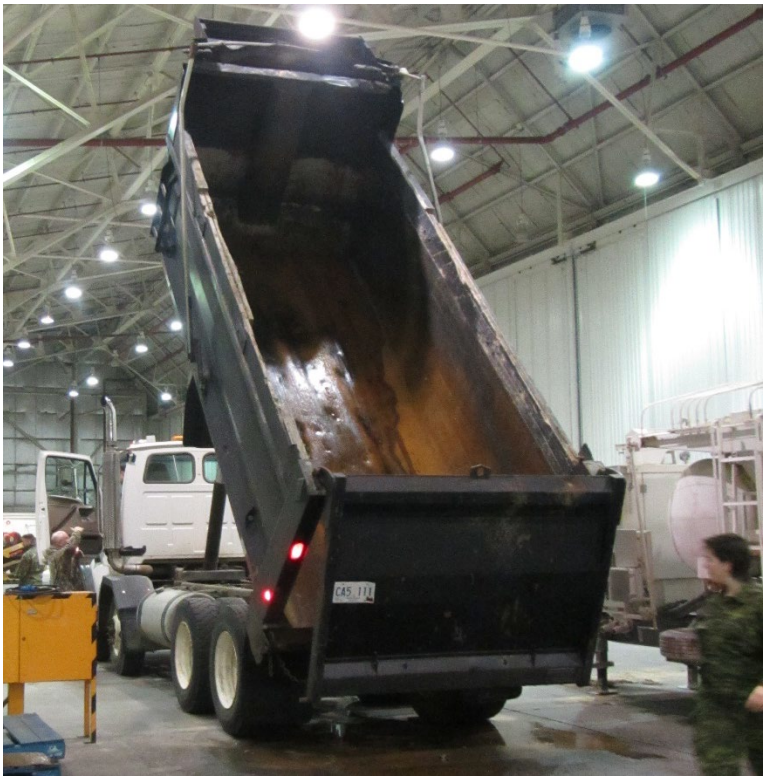

3.2.6 Water Tank

A 2,000 or 3,000 gal. water truck is typically used during RADR operation for flowable fill dry method placement and for refilling the SVM supply tanks. However, since a water truck was not available for rent, 250 gal. plastic totes were used (Figure 23). A ball valve located at the bottom of the tank was used to connect 2 in. diameter hoses via cam lock. The water tanks were also used to apply water during mixing of the snow-water slurry.

Figure 23. Plastic totes used for water supply.

3.2.7 Plate Compactors

A Wacker Neuson VPG 160B vibratory plate compactor (Figure 24) was used for compaction when backfilling geocells filled with sand. The walk-behind plate compactor weighed 169 lb and produced a centrifugal force of 3,968 lbf. The plate size was approximately 1.77 ft by 1.38 ft. For compacting the processed snow, a heavier plate compactor, the Wacker Neuson BPU3050 (Figure 25), was used. Specifications for this heavier model are provided in Table 7.

Figure 24. Wacker Neuson VPG 160B vibratory plate compactor.

Figure 25. Wacker Neuson BPU3050 plate compactor.

Table 7. Wacker Neuson BPU3050 specifications.

Specification	Value
Operating Weight (lb)	376
Centrifugal Force (lbf)	6,750
Base Plate Thickness (in.)	0.4
Height (without Guide Handle)	27.5
Operating Height (Adjustable Guide Hand Down, in.)	31.5
Operating Height (Adjustable Guide Handle Up, in.)	45
Operating Width (in.)	19.7
Frequency (Hz)	90
Advance Travel (ft/min)	68.9
Motor Type	Air-cooled, single-cylinder 4-cycle engine
Motor Manufacturer	Honda
Motor Model Number	GX270
Avg Fuel Consumption (gal./hr)	3
Tank Fuel Capacity (qt)	5.3
Fuel Type	gasoline

3.2.8 Vibratory Roller Compactor

A small, ride-on vibratory compactor (Figure 26) was used to compact snow-water slurry and sand backfill materials once the material had been placed so that it was level with the surrounding pavement to ensure adequate density near the surface of the repair. A Caterpillar CS34 model (Figure 26) was used. Table 8 shows the specifications of this compactor.

Figure 26. CS34 vibratory compactor.

Table 8. Caterpillar CS34 vibratory compactor specifications.

Specification	Value
Engine Model	CAT® C3.4B
Maximum Gross Power (hp)	74
Operating Weight (lb)	9,799
Maximum Travel Speed (mph)	5.5
Height, with Cover (in.)	98
Width, Overall (in.)	54.5
Length, Overall (in.)	164.5
Drum Width (in.)	50
Drum Diameter (in.)	40
Vibration Frequency (Vibrations per min)	2,100

3.2.9 Simplified Volumetric Concrete Mixer

A customized, tow-behind SVM (Figure 27), manufactured for the RADR program by ProAll in consultation with ERDC, was used for capping the repairs with RSC. The SVM is precalibrated for rapid-setting cementitious repair materials to include RSFF and RSC capping material. The mixer was moved around the site via a dump truck with a pintle hook trailer connection.

Figure 27. Simplified Volumetric Mixer (SVM).

The mixer consisted of a single dry material hopper with a capacity of approximately 7 yd^3, a conveyor belt feed system, a positive displacement water pump to meter the mix water according to fixed pump speed, two 200 gal. water containers on each side of the mixer, a washout container with a pressure washer, and a replaceable mixing auger. The machine was outfitted with two retractable catwalk platforms, a bin entry platform, a replacement auger, and two super sack piercing points. A steel grate was located near the bottom of the dry material bin to prevent large pieces of material, from entering the conveyor belt and possibly causing considerable damage.

3.2.10 Concrete Finishing Tools

A 12 ft long magnesium bar screed (Figure 28) was used to strike off crater repairs capped with RSC. Finishing was kept to a minimum to comply with standard RADR practice. However, hand trowels were used to ensure the edges of the repair were clean, as excess repair material that spills onto the parent slab and is allowed to cure can create FOD potential.

Figure 28. Magnesium bar screed.

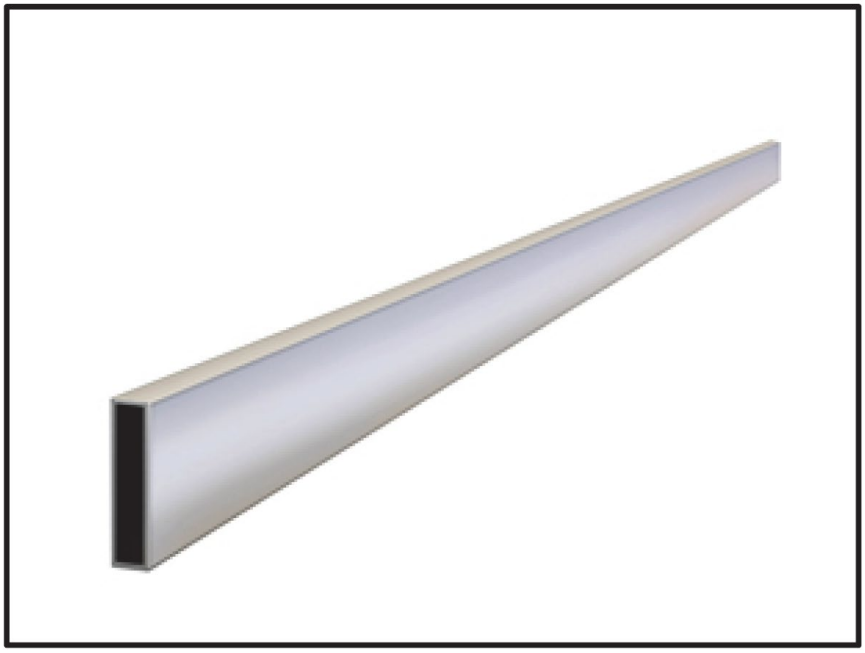

3.3 Materials

3.3.1 Snow

All nonlegacy patching was performed by using natural snow harvested from areas immediately adjacent to the test site (Figure 29). This snow presented as tall, roughly triangular cross-section banks along the northern and southern edges of the test site (Figure 29). This snow had been plowed from the large test site area. The snow had an unknown age, but its cleanliness was good (minimal foreign materials present). It had not been through multiple thermal cycles that reached temperatures higher than about 25°F (evidenced by mostly angular ice grains and limited spherical particles). It was lightly bonded (ice grain to ice grain connections) so that it broke loose in clumps when excavated by a loader bucket but easily disaggregated when placed under minimal compressive force.

Figure 29. Snowbanks along north side of test area used as patching material for snow-based crater repairs.

Natural snow on the ground at the time of testing was 17.5 in. deep with a temperature of 3°F on the surface and 21°F at the interface with a grassy soil terrain. Table 9 summarizes the stratigraphic profile of this snow. Owing to stable midwinter weather present in Goose Bay for some time prior to the onset of our testing, we can assume that the snow from the banks along the test site that were used for patching originally possessed similar properties.

Table 9. Natural undisturbed snow present adjacent to work site at time of testing.

Layer (in.)	Density (lb/ft^3)	Snow Description
0–4	10.6	0.04–0.06 in. crystalline angular ice grains with limited bonding
4–8	16.2	thin ice lens at top boundary; 0.06–0.08 in. crystalline slightly rounded ice grains with moderate bonding
8–12	17.5	same as above
8–17	23.1	0.08 in. mostly rounded ice grains with little to no bonding (trending toward depth hoar)

When the test protocol called for patching with a slurry, water was added to the borrow snow at the point where the snow was placed near the crater

in preparation for the repair process. Water was added at a nominal quantity of 25 gal./cu yd (Figure 30). Mixing was accomplished using a snowblower (Section 4.1) in the process of placing snow in the repair (Figure 31).

Figure 30. Adding water to harvested snow.

Figure 31. Snowblower mixing wetted snow and ejecting it into the crater in preparation for manual leveling and compacting in prescribed lifts.

3.3.2 Cellulose Additive

Laboratory tests have shown that the strength of a frozen snow-water slurry is significantly greater when a small amount of cellulose is added (Asenath-Smith et al. 2019). While it is easier to produce a uniform cellulose-water-snow mixture in the laboratory, we sought to test the impact of this additive in a field setting. Cellulose from 40 gal. drums was added to the snow by manual shoveling immediately after water was added (Section 4.6.1). The drummed material was a viscous cellulose-water mixture. The target concentration was 4 gal. of drummed cellulose per cu yd. Mixing was achieved with the snowblower (Section 4.6.1) at the same time water was being mixed with the snow and placed in the crater.

3.3.3 Sand

Locally available sand was also used as a backfill material. The material classified as a poorly graded sand (SP) according to the Unified Soil Classification System (USCS) described in ASTM D2487 (2017a). A plot of the grain size distribution can be found in Figure 32. Backfill sand would traditionally be stockpiled and transported with a dump truck to the repair site where it would be placed with a front-end loader or CTL. However, for this test the material was provided in bulk super sacks (Figure 33) so that is could be neatly stored indoors to prevent the material from freezing. The temperature of the sand measured at the time of testing was approximately 59°F.

Figure 32. Backfill sand grain size distrubtion.

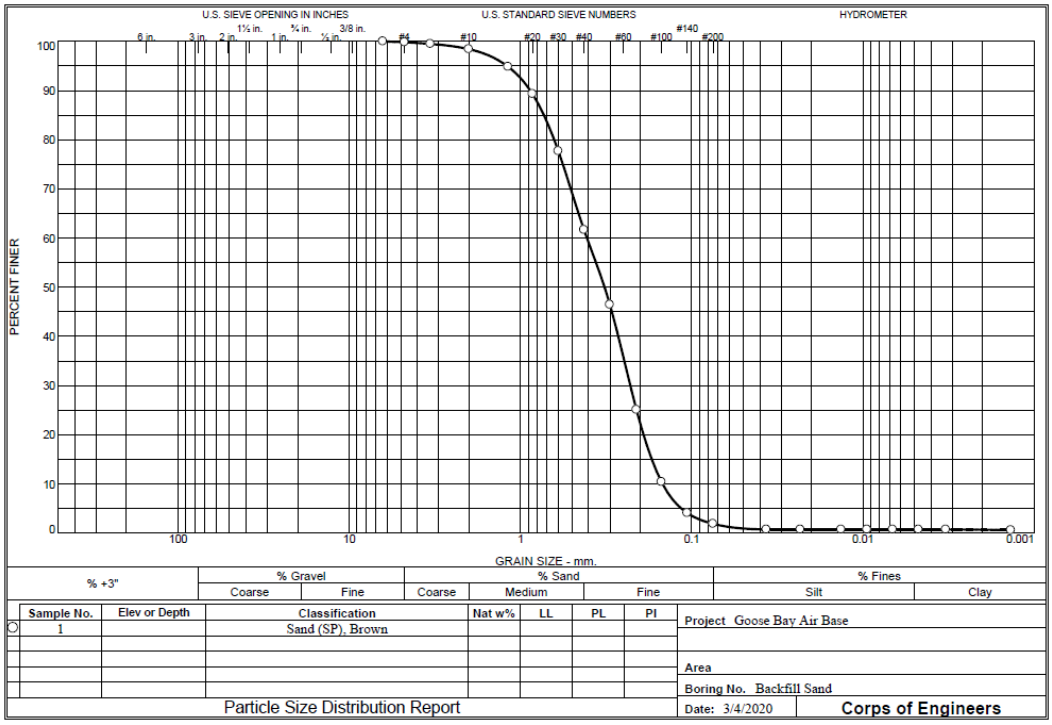

Figure 33. Super sack of sand material.

3.3.4 Geocells

A geocell, formerly known in the community as a "sand grid," is a geosynthetic cellular confinement system with interconnected cells used to reinforce geotechnical materials, mostly cohesionless soils. Within the scope of RADR, geocells are used to reinforce backfill materials for expedient crater repairs. One of the primary benefits of using geocells is that lower quality backfill materials can be used rather than the traditional well-graded crushed limestone material.

For this study, GeoProducts Envirogrid EGA208PT (Figure 34) was used. The geocells were made from HDPE material that was ultrasonically welded together. The cells were 8 in. tall and came in 8.4 ft × 21.4 ft sections, which were cut to fit inside the excavated repairs. Once expanded, the approximate cell dimensions were 8.8 in. × 10.2 in. with a weld spacing of 14 in. Additional information concerning Envirogrid GA208PT and several other brands of geocells can be found in Garcia et al. (2021). The installation procedure used for this report can be found in Section 4.6.2.

Figure 34. GeoProducts Envirogrid EGA208PT geocells.

3.3.5 Rapid-Setting Flowable Fill (RSFF)

In general, traditional flowable fill is a low-viscosity, grout-like cementitious blend commonly composed of portland cement, fine aggregate, and water. RSFF uses calcium sulfoaluminate (CSA) cement to

provide a much faster set time than traditional flowable fill. The dry materials are stored in large 3,000 lb super sacks fashioned from woven geotextile fabric and lined with plastic. The preblended material requires only the addition of water to conduct repair activities. The product used for the testing described in this report was Fastrac Fastfill manufactured by Western Design and Materials, LLC (Figure 35). The RSFF was stored inside for approximately 72 hr before testing. During testing, the temperature of the RSFF material was 9°F.

Figure 35. Fastrac Fastfill rapid-setting flowable fill (RSFF).

RSFF was selected for RADR operations because it can be placed expediently without the need of mixing equipment by using the placement technique known as the "dry method" (Priddy et al. 2013a; 2013b). In this method and for this experiment, thin 4 in. to 6 in. thick lifts of dry material were placed in the excavated repair, and then approximately 40 to 50 gal. of water was applied to the surface of each lift and allowed to percolate through the dry material. The material generally provides a UCS of 250 psi after 30 min of cure time and 750 psi after 3 hr of cure time. Post-trafficking investigations typically reveal a CBR of approximately 100 percent after 24 hr of cure time. A full laboratory characterization of RSFF can be found in Carruth (2020). RSFF was used as a backfill for FRP matting and RSC during full-scale experiments.

3.3.6 FRP Matting

The FRP matting system (Figure 36) functions as a modular FOD cover for RADR and consists of four panel types of differing sizes:

- Full-size panel (208 in. × 78 in.)
- Half-size panel (108 in. × 78 in.)
- Full-size anchor panel (200 in. × 24 in.)
- Half-size anchor panel (100 in. × 24 in.)

Panels are approximately 0.4 in. thick with an approximate unit weight of 3.6 lbm/ft^2 and are joined with connector bushings to form a cover to be placed over a backfilled crater and anchored to existing pavement by approved anchoring systems. Full- and half-size panels have two adjacent edges recessed at the panel bottom and the two remaining panel edges recessed at the panel top, yielding two "overlap edges" and two "underlap edges." Lower joining bushings are preattached to receiving holes located on the underlap edges of full- and half-size panels. Anchor panels are necessary to facilitate the transition from full- and half-size panel underlap edges to open holed edges for anchoring and are intended to be placed on the leading edge of the repair with respect to the primary direction of flight. Additional details regarding the FRP matting system and its development can be found in Rushing et al. (2016a, 2016b). Specific installation details regarding the testing described in this report can be found in Section 4.7.1.

Figure 36. Assembled fiber-reinforced polyester (FRP) matting system.

3.3.7 RSC

The RSC used for this experiment was CTS Rapid Set Concrete Mix® (Figure 37), which is a rigid capping material used in RADR scenarios because of its high early strength and load-carrying capacity after a minimal curing time. The preblended material consists of cement, fine aggregate, and coarse aggregate and requires only the addition of water to be placed. CTS Rapid Set Concrete Mix® has a fast set time of 20 to 30 min, depending on the air temperature. The main cementitious component in the mix is CTS's proprietary RapidSet Cement®, a CSA-based material. The coarse aggregate included in the mix is 3/8 in. maximum size pea gravel. The dry blend of cementitious material and aggregate is stored in large 3,000 lb super sacks composed of woven geotextile. The RSC material used for testing was received and stored for 12 hr inside before testing, at which time the temperature of the material was 16°F.

The material was mixed and placed using the USAF SVM. The material is placed in a manner similar to the placement of ordinary concrete, but it must be placed expediently, since it begins to harden and set more rapidly than conventional concrete.

Figure 37. CTS Rapid Set Concrete Mix® rapid-setting concrete (RSC).

4 Repair Process, Training Procedures, and Training Results

The general crater repair process is the same regardless of the type of equipment or repair materials used to conduct the repair. The process is well described in Edwards et al. (2013); Bell et al. (2013); Bell et al. (2018); and Carruth et al. (2015) and consists of the following tasks: (1) initial debris removal, (2) marking, (3) hauling of materiel, (4) pavement cutting, (5) breaking and excavating, (6) backfilling, (7) capping, and (8) final debris removal. This chapter describes how each of these processes was carried out for the various repairs conducted as a part of this experiment.

4.1 Initial Debris Removal

The first task for repairing craters was debris removal. The debris removal team consisted of two airmen, one operating a front-end loader and one operating a CTL with a bucket attachment. To train for this activity, the airmen were shown how to use the equipment controls.

The debris removal team began the crater repair process by clearing the path from the staging area to the minimum operating strip (MOS) and then removing debris from each crater to be repaired in sequence. The team also removed debris as it was excavated from each repair and moved it to the sides of the MOS. The debris removal team consisted of two personnel operating a front-end loader and a CTL with a bucket attachment. To train for this activity, the airmen were shown how to use the equipment controls; and debris generated from training craters was moved to the side of the repair area. Figure 38 shows photos of debris removal with a front-end loader.

Figure 38. Debris removal with front-end loader.

4.2 Marking

The marking team consisted of three airmen that used line-of-sight stanchions to identify the crater upheaval. Stanchions consist of two sighting stands placed outside the upheaved area and a target rod that is systematically moved between the stanchions to determine where the upheaved pavement begins and ends. Additional details regarding stanchions can be found in Technical Order (T.O.) 35E2-5-1 (USAF 1992).

For this experiment, no upheaval was present because craters had not been generated via actual explosives, so the marking team marked the extent of the repair area by using a straightedge with a lumber crayon. Spray paint can also be used but was avoided due to the cold temperatures. Repair sizes were set to a nominal dimension of 10 ft × 10 ft.

4.3 Hauling

The haul team consisted of three airmen, including a dump truck operator, a telehandler operator, and a spotter. While marking was being conducted, transport of equipment, tools, and repair materials from the warehouse to the repair site began. The primary repair materials requiring dedicated haul team assets included the super sacks of sand, flowable fill, and RSC, which were hauled from the storage site to the repair site. The repair materials and supplementary equipment are typically loaded onto a flatbed trailer pulled by a prime mover with sufficient capacity. However, a

flatbed trailer was unavailable for this experiment, so material was transported in the dump truck with the end gate removed.

4.4 Pavement Cutting

The saw-cutting team consisted of two airmen: the saw operator and a spotter (Figure 39). Pavement cutting began once the marking team completed its duties. The current USAF pavement cutting protocol calls for four wheel saws attached to CTLs to cut the upheaval of two craters simultaneously; each wheel saw cuts two lines per repair. A walk-behind saw using a diamond blade can be used in locations where dowel bars are present.

For this experiment, only one CTL with a CAT SW360 wheel saw was used due to equipment limitations and the small number of crater repairs to execute each day. The spotter ensured proper alignment of the saw before and during cutting and cleared away concrete dust generated by the saw.

Figure 39. Pavement cutting with CTL, saw attachment, and spotter.

4.5 Pavement Breaking and Excavation

The excavation team consisted of two airmen to operate the excavators and two spotters. The breaking and excavation teams were responsible for breaking up the damaged PCC within the cut crater repair area and removing the disturbed subsurface material. An excavator with a hammer attachment was used for breaking any large sections of the existing pavement within the repair area, and a second excavator with a bucket attachment was used for removing the broken pavement and disturbed

underlying material. Figure 40 shows pavement breaking with a CAT 329D excavator. Photos of excavation can be found in Section 3.2.2 of this report.

Figure 40. Pavement breaking with CAT 329D excavator.

4.6 Backfill

Once the repair was excavated, backfill was placed to prepare for the surface material. For this experiment, multiple backfill materials and procedures were used. Each of these is described in the following sections.

4.6.1 Snow-Water Slurry and Snow-Water Slurry with Cellulose

Before snow can be used as a backfill material, the level of moisture must first be assessed. The snow will be either ideally moist, drier than ideal, wetter than ideal, or saturated. The processing procedure varies depending on the level of moisture. The most common condition encountered naturally is drier than ideal, which was the condition of the snow used for this experiment. The procedure for processing drier than ideal snow is described in the following paragraphs. Procedures for processing any of the moisture conditions can be found in Appendix B.

The snow was first obtained from the stockpile and placed near the repair with a front-end loader (Figure 41). Before water was added, the snow was processed with a snowblower and CTL attachment to remove any existing clumps (Figure 42). Next, water was added to the stockpile at a rate of approximately 33 gal./cu yd via the water source (Figure 43). Subsequently, the snow was processed again with the snow blower attachment. During the

second period of mixing with the snow blower, the snow was directed towards the repair to minimize moving the snow by hand.

Figure 41. Placing snow from stockpile adjacent to repair.

Figure 42. Processing stockpiled snow with snowblower attachment.

Figure 43. Adding water to snow to achieve ideal moisture.

The processed snow was then spread evenly within the repair before compaction. Preferably, only the quantity of snow needed for one lift was processed each time. The volume of borrow snow required was approximately 1.5 times the volume of the finished lift. Table 10 shows the target lift thickness for repairs backfilled with snow.

Table 10. Recommended lift thicknesses for compacted snow.

Lift	Placed t[a] (in.)	Compacted t[a] (in.)
Initial	10	7
Second through penultimate	7	5
Final (top)	6	4

[a] t = thickness

Immediately after leveling, the snow was compacted using two coverages of a plate compactor. A coverage is defined as the compactor applying compaction to every location within the repair. For the final lift, the material protruded approximately 2 in. above the surrounding pavement. Instead of compacting immediately, the material was allowed to harden before final compaction with the vibratory roller. Hardening time varies depending on temperature, but 1 hr was used for this experiment.

Figure 44. Compaction of final lift of snow-water slurry with vibratory roller compactor.

4.6.2 Sand-Filled Geocell

For repairs backfilled with sand-filled geocells, the excavation depth was approximately 17 in. Two layers of the geocell were used, and each layer was approximately 8 in. thick, so the 17 in. accounts for both layers plus a 1 in. thick buffer. The goal was to install the geocells such that they were approximately level with the surrounding pavement after final compaction.

Before geocell installation, the existing subgrade was compacted with two coverages of a rammer-style compactor. A coverage is defined as moving the compactor across the entire compacted surface one time, which typically occurs starting in one corner of the repair and moving towards the center in a circular pattern. If the excavation depth was too deep, sand was added and compacted with two coverages of the plate compactor until a repair depth of 17 in. had been reached. Next, a layer of needle-punched, nonwoven geotextile was installed (Figure 45).

Figure 45. Geotextile installed below geocell layers.

Once the exact plan dimensions of the repair were determined, the geocells were cut to fit. A proper fit is critical since expansion of the cells is needed for optimal performance. In cases where the repair length was different from the repair width, the dimensions of the first layer of geocells may not be the same size as the sections for the second layer, because the top layer was placed transverse to the bottom layer. The simplest method was to drive a piece of rebar (or similar) in the ground in a square of the same dimensions as the repair, or hold the corners open with a piece of scrap lumber or the handle of a shovel if measuring on a hard surface (Figure 46). Each of the rebar stakes or handles represented the corners of the repair. An additional piece of rebar or a handle was placed between these to prevent the geocell section from collapsing. To cut the first layer of geocells, the corners of a geocell section were placed at two of the corners and then expanded in the direction of traffic (since the first geocell layer is expanded parallel to the direction of traffic.). While fully expanded, the excess length of the geocell section was trimmed using a utility knife (Figure 47). Each cell was cut individually and carefully such that excess material was not cut. The procedure was repeated for the second layer, except the geocells were expanded perpendicular to the first layer.

Figure 46. Expanding geocells inside repair.

Figure 47. Cutting geocells to proper length.

Once the geocells were cut to the appropriate size and placed into the repair, super sacks of sand were lifted over the repair with the telehandler, the bottom of the super sack was cut with a utility knife, and the sand was leveled with rakes as it fell into the repair. Sand was placed until a level of approximately 1 in. above the top of the geocells was reached. The plate compactor was used to compact the first layer (Figure 48).

Figure 48. Compaction of first layer of geocell backfill.

4.6.3 RSFF

For RSFF backfill dry method placement, a target thickness of 14 in. was used to match the standard thickness in the interim RADR TTPs recommended by the USAF. The typical dry placement method was used, which involved lifting a super sack over the repair and cutting the bottom to allow dry material to fall into the repair (Figure 49). The dry material was then spread evenly with hand tools (Figure 50), and 40 gal. of water was metered evenly over the surface and allowed to percolate through the material (Figure 51). Another super sack of material was brought in, and the process was repeated until the target thickness was reached. If partial super sacks were required, the amount of water used was adjusted

accordingly. Only 25 gal. of water was used for the final super sack to limit the amount of standing water on the backfill surface.

Figure 49. Placement of dry RSFF.

Figure 50. Leveling dry RSFF with hand tools.

Figure 51. Dispensing water over dry RSFF.

4.7 Capping

After backfilling operations were complete, repairs were capped either with the FRP matting system or RSC before trafficking. The following sections describe the procedure for installing FRP and placing RSC.

4.7.1 Fiber-Reinforced Polyester (FRP) Matting

Hands-on field training was provided to familiarize troops with the assembly and anchoring of the FRP matting system in accordance with the USAF interim process for FRP matting installation and maintenance actions. The FRP panels were first transported and assembled near the crater repair location. For all repairs capped with FRP, one full panel and two half panels were used, resulting in a repair area of 18 ft × 13 ft.

The primary direction of flight was selected to ensure that the assembled FRP cover would overhang at least 1 ft onto sound pavement, and then the assembled cover was checked for skewness. Next, the anchor locations were checked to ensure that anchors would not fall within 6 in. from a PCC joint or medium- or high-severity crack. Repair team members were instructed to use hand tools to clear the immediate area surrounding the repair of remaining debris and use push brooms to sweep fine debris away from the repair so as not to trap FOD between the FRP mat and the pavement surface. Assembly consisted of placing the overlap portion of the panels over the underlap and tightening the joining bushings with impact wrenches.

The FRP field training proceeded as described in the steps below:

1. Team members placed the first panel of the FRP assembly on the right-hand side of the repair's trailing edge such that the overlap-overlap corner of the panel was on the right-hand side.

2. If necessary, depending on repair width, the next FRP panel was placed to the left of the first panel such that its overlap edge was atop the first panel's underlap edge.

3. If necessary, team members made small, manual adjustments to the position of the second panel so that the holes in the overlapping edge of panel #2 aligned over top of the lower joining bushings in the underlapping edge of panel #1.

4. Once the desired repair assembly width was achieved, repair team members were trained to begin placement of the second row of FRP panels beginning on the right-hand side of the repair and proceeding leftwards in a brickwork fashion so that no longitudinal joints in adjacent rows of the FRP assembly fell in line with each other and the holes in the overlapping panel edges aligned with the lower joining bushings in previously placed panel underlap edges.

5. Connector bushings were installed hand-tight in the longitudinal joint in the first row of panels (if present). Then, connector bushings were installed hand-tight in the transverse joint between the first and second rows of panels.

6. For this experiment, a third row of FRP panels was not typically required. The repair team members were instructed to place a row of anchor panels on the leading edge of the repair while continuing to conform to the brickwork assembly style (Figure 52).

7. Connector bushings were installed hand-tight in the transverse joint to connect the anchor panel(s) to the underlapping edge of the previous row of assembled FRP panels.

8. Team members were trained to tighten all connector bushings by using an electric impact wrench with 15/16 in. socket (Figure 53) and to ensure final torque with a torque wrench with 15/16 in. socket and resistance set to 110 ft-lbf.

9. Prior to the initiation of the anchoring process, the capping team leader (or crater chief) was trained to make a judgment determination as to whether the assembled cover was within the allowable skewness limit of less than 5° and to adjust the position of the entire cover as necessary.

10. Then, team members were trained to install the PowerBolt+ PCC anchors along **only** the leading and trailing edges of the FRP cover beginning from one side of the cover and proceeding sequentially across without skipping any anchor holes as follows:

    a. Use the open hole in an anchor bushing as a guide and an electric hammer drill with ¾ in. diameter carbide bit to drill to the target depth while a spotter ensures that the drill is plumb from both a longitudinal and transverse perspective (Figure 54). The target depth was 9 in., and a piece of tape was used to mark the drill bit as a depth indicator.

    b. Use an air compressor with wand to blow dust and debris from the anchor hole while making sure not to trap debris between the FRP mat and the pavement surface.

    c. Place the anchor bushing back atop the anchor hole and sink the PowerBolt+ anchor full depth into the anchor hole with a 3 lbm engineer's hammer or sledgehammer.

    d. Deploy and tighten the anchor with an electric impact wrench and a 15/16 in. socket.

    e. Ensure final torque with a torque wrench with 15/16 in. socket and resistance set to 110 ft-lbf (Figure 55).

Figure 52. Installation of FRP anchor panel.

Figure 53. Tightening of FRP connector bushings with impact wrench.

Figure 54. Drilling anchor hole with spotter.

Figure 55. Final torque check on installed anchor.

4.7.2 Rapid-Setting Concrete (RSC)

To begin the capping process, the SVM was prepared for standard operation. Super sacks of dry RSC mixture were loaded into the dry material bin (Figure 56), the mix water and washout tanks were filled, and the mix auger and concrete tools were sprayed with concrete release agent. The water pump gear controls were set to "Rapid Set," which is the lower gear. The SVM is previously factory calibrated to provide the optimum amount of water for RSC (approximately 50 gal./cu yd at a gate setting of 6).

To dispense material, the conveyor belt and water pump controls were turned to the "ON" position. Sufficient material was placed and distributed evenly by using hand tools. The material was struck off by using a magnesium bar screed (Figure 57), and any excess material was removed from the edges using trowels as necessary. Immediately after placement was completed, the mixer was washed out using the onboard or external pressure washer.

Figure 56. Loading super sacks into dry material bin.

Figure 57. Striking off RSC with magnesium screed bar.

5 Test Results and Discussion

After several training repairs were conducted, two full-scale experiments were conducted using the crater repair equipment and materials described in Chapter 3 and the procedures described in Chapter 4. Table 11 shows the repair names along with their backfill and cap types. The first repair is designated repair T1 or "Training 1," since it was used as a training crater, but unlike the other training craters, characterization data were collected on it for several days.

Table 11. Compacted snow-water slurry repair details.

Repair #	Backfill	Surface	Date
1	Frozen water	None	21 January 2020
2	Compacted snow-water slurry	FRP	25 January 2020
3	Compacted snow-water slurry	None	25 January 2020
4	Compacted snow-water slurry with cellulose	None	25 January 2020
5	Sand-filled geocell	FRP	31 January 2020
6	RSFF	FRP	31 January 2020
7	RSFF	RSC	31 January 2020

The two full-scale experiments were conducted on separate days and consisted of timed three-crater sequences. The first experiment involved use of new methods involving compacted and snow and ice (Repairs 2, 3, and 4), while the second experiment used existing RADR crater repair methods (Repairs 5, 6, and 7). The dates of each of the two experiments are included in Table 11, and the hourly weather data for each event can be viewed in Appendix A.

Although timing data were collected, it is not recommended for direct comparison to previous tests or standard RADR task times provided in the interim RADR TTPs, because the standard team sizes and equipment quantities were not used. The total team size was 16 airmen.

During the time Repairs 2, 3, and 4 were conducted (25 January 2020), the ambient temperature ranged from 10°F to 18°F, with a wind chill ranging from –7°F to 6°F. During the curing period over the next 48 hr, the ambient temperature increased up to 25°F the following day, before falling back to between 10°F and 14°F two days later. Repairs 5, 6, and 7 were conducted on 31 January 2020, and ambient temperatures ranged from 12°F to 19°F with wind chills between –1°F to 4°F. After RSFF and

RSC placement, the temperature began falling overnight, down to 1°F the following morning with a minimum wind chill of –15°F.

5.1 Repair Timing Results and General Observations

Three repairs were conducted using compacted snow and ice-based methods. Table 11 shows the repair names and repair materials used. Because craters were not created from actual charges, initial debris removal and upheaval detection were omitted. The first step was to make the extent of the repairs, which was fixed at 8.5 ft × 8.5 ft. The airmen elected to mark only the corners of the repairs, which aligns with the current draft RADR TTPs. Lumber crayons were used to mark the repair instead of spray paint due to the freezing temperatures. Timing data were recorded for some of the crater repair tasks. These timing results, along with a discussion of the results, are provided in the following sections.

5.1.1 Saw Timing Results

Table 12 shows pavement cutting results collected for some repairs. The CAT SW360 saw attachment described in Section 3.2.1 was used for all pavement cutting performed. During training, we observed that the only way for the saw operator to complete cutting was to do so in three separate plunges rather than a continuous forward cut. A layer of ice on the surrounding pavement prevented adequate traction for a single plunge and continuous cut. Accordingly, the time of each plunge, as well as the total cutting time, was recorded and included in Table 12.

The calculated cut rates ranged from 0.30 to 0.55 ft/min, which is much less than those reported by Bell et al. (2019) when similar saw attachments were used. In addition, several teeth were broken during the cutting of each repair. For Repairs 3, 4, 5, and 6, a total of 6, 6, 15, and 20 teeth, respectively, were replaced during cutting. Breaking of large quantities of teeth has not occurred in any of the previous saw-cutting work performed by ERDC.

Table 12. Pavement-cutting test results.

Repair #	Cut #	Time (min)				Cut Length (in.)	Cut Rate (ft/min)
		Plunge 1	Plunge 2	Plunge 3	Cut Total		
3	1	5.25	6.00	7.00	18.25	—	—
—	2	6.50	7.00	7.50	21.00	—	—
—	3	7.50	8.25	12.00	27.75	—	—
—	4	9.17	8.50	5.25	22.92	—	—
4	1	5.50	6.50	5.25	17.25	—	—
—	2	6.50	7.25	5.00	18.75	—	—
—	3	7.75	7.50	6.00	21.25	—	—
—	4	6.50	7.50	6.00	20.00	—	—
5	1	3.50	5.47	7.82	16.79	111	0.55
—	2	9.98	7.30	5.97	23.25	115	0.41
—	3	10.07	6.82	5.48	22.37	111	0.41
—	4	9.55	8.13	6.77	24.45	117	0.40
6	1	8.92	6.43	6.93	22.28	98.5	0.37
—	2	11.03	8.78	7.92	27.73	100	0.30
—	3	8.87	7.63	11.50	28.00	100	0.30
—	4	7.15	7.13	3.93	18.21	95	0.43

5.1.2 Breaking and Excavation Observations

Specific timing results were not recorded for breaking and excavation because this task was conducted over several days in many cases, and some repairs were reused to reduce the number of open excavations on the site (i.e., excavation was performed on repair materials instead of existing PCC pavement). Initial breaking was typically completed during training activities. General observations concluded that breaking and excavating proceeded as they would in a moderate climate. Since the large excavator was stored outside each night, an electrically powered block heater was used to enable prompt engine start at the beginning of the workday. The CAT 329D was preferred for breaking, since it was a larger, more powerful machine; but the CAT 308E was preferred for excavation due to increased maneuverability.

5.1.3 Backfill Timing Results

Backfill timing results are provided in Table 13. Repair 2 and Repair 3 have similar results as expected, since the same backfill type was used. The use of the cellulose additive could have contributed to the increase in time required to backfill Repair 4.

Repairs 2, 3, 4, and 5 took similar amounts of time to backfill, while Repair 6 took the most time to backfill. This increase could be due to the limited training provided for RSFF backfill, a material with which the airmen were generally unfamiliar. Repair 7 took much less time than Repair 6, because the target thickness of flowable fill was much less (14 in. versus 24 in., respectively). Repair 7 took much longer than the 11 min allotted by the interim RADR TTPs, which was likely due to lack of training. The extremely cold environment could also have been a factor.

Table 13. Backfill timing results.

Repair #	Backfill Type	Total Backfill Time (min)
1[a]	Frozen water with debris	n/a
2	Compacted snow-water slurry	47
3	Compacted snow-water slurry	51
4	Compacted snow and ice with cellulose	63
5	Sand-filled geocell	69
6	RSFF	102
7	RSFF	44

[a] Repair 1 was a training repair, so backfill time was not recorded.

5.1.4 Capping Timing Results

Capping timing results for some repairs are displayed in Table 14. Repairs 1, 3, and 4 were not capped, and a capping time for Repair 2 was not recorded. Repairs capped with FRP (5 and 6) took on average 59 min to cap. Typically, these size repairs take only approximately 30 min to cap with FRP. The inexperience of the airmen, along with the extremely cold environment, could have caused the longer than expected installation times. Repair 7 took only 10 min to cap with RSC, which met the capping time requirement of 11 min listed in the interim RADR TTPs.

Table 14. Capping timing results.

Repair #	Cap Type	Total Capping Time (min)
5	FRP	66
6	FRP	52
7	RSC	10

5.2 Trafficking Description and Results

To determine the structural capacity of the repairs, a single-wheel C-17 load cart was used (Figure 58). The cart was loaded to produce an approximate wheel load of 45,000 lbf with a tire pressure of 142 psi. The

cart was operated normally despite the cold conditions, with the exception of using sand around the repairs periodically in order to gain sufficient traction. Due to the relatively small size of the repairs, a channelized traffic pattern was used, where traffic was applied down the center of the repair from west to east, and then the cart was reversed.

Figure 58. C-17 single-wheel load cart.

Data collection was performed periodically during trafficking. First, visual observations were conducted, and any damage to the repair surface was noted. Rut depths were measured by placing a 10 ft long straightedge across the repair transverse to the traffic direction in the center and at the two quarter points. The maximum rut depth was recorded in each instance, with a 3 in. deep rut considered as failure. For repairs surfaced with FRP matting, the front tire of a front-end loader was employed to deflect the FRP matting downward along the profile of the rut basin in the underlying material (Figure 59).

Figure 59. Typical rut depth measurement.

Traffic was applied to Repair 2 48 hr after final compaction. Table 15 shows rut depths measured for Repair 2. Rutting progressed rapidly during the first 30 passes, then slightly slowed and appeared to stabilize by 80 passes. When trafficking had reached the 100-pass target for an expedient repair, it had not exceeded the failure criteria of 3 in. The FRP was removed, and rut depths were measured on the snow slurry backfill surface (see *note b* in Table 15). A limited area along the traffic path displayed disaggregated snow typical of failed and disturbed snow.

A patching procedure was then conducted to develop TTPs for a damaged snow slurry backfill. The disturbed snow was removed, and a small batch of fresh borrow snow and water were mixed in place. The small patch was compacted using a vibratory plate compactor and left to cure for 12 hr. The following day, characterization data collected with the Russian Snow Penetrometer (RSP) results indicated that the patch could sustain traffic. RSP use and data collection are discussed further in the next section.

FRP was reinstalled, and trafficking resumed. Periodic rut depth data collection was performed (see *note c* in Table 15). As shown, rutting after another 100 passes was much less than that measured just before the patch was conducted.

Table 15. Repair 2 rut depth data.

Pass # — TOTAL	Maximum Rut Depth (in.)		
	East[a]	Center[a]	West[a]
0	0.24	0.60	0.12
10	0.36	0.84	0.36
20	0.60	1.08	0.72
30	1.20	1.20	0.72
50	1.32	1.32	0.72
80	1.56	1.56	0.84
100	1.56	1.56	0.84
100-mat removed[b]	1.08	2.40	0.72
110[c]	0.48	0.36	0.36
120[c]	0.24	0.36	0.36
150[c]	0.36	0.43	0.48
200[c]	0.36	0.60	0.60

[a] East, center, and west refer to the data collection locations across the repair.

[b] Measurements conducted on backfill surface after FRP removal.

[c] Patching was conducted after 100 passes. All these measurements were conducted after patching.

Trafficking of Repair 3 began 48 hr after final compaction, and rut depth data are displayed in Table 16. A small amount of rutting was established quickly, within the first few passes, and then remained virtually unchanged for the remainder of trafficking. Occasionally, rutting was observed to decrease slightly, which was likely due to slight variation in measurement between data collections. Trafficking continued to 500 passes with observations and periodic measurements confirming that insignificant additional rutting occurred under traffic.

Table 16. Repair 3 rut depth data.

Pass # — TOTAL	Maximum Rut Depth (in.)		
	East[a]	Center[a]	West[a]
0	0.24	0.84	0.48
10	0.36	0.84	0.72
20	0.36	0.84	0.72
30	0.60	0.84	0.72
50	0.60	0.84	0.72
80	0.60	0.84	0.72
100	0.60	0.84	0.72
110	0.48	0.60	0.84
120	0.48	0.72	0.48
150	0.48	0.72	0.36
200	0.36	0.72	0.60
500	0.48	0.72	0.60

[a] East, center, and west refer to the data collection locations across the repair.

Repair 4 cured for 72 hr before trafficking, because RSP results indicated that sufficient strength had not yet developed to allow trafficking after 48 hr of curing. Rut depth measurements for Repair 4 can be found in Table 17. After 100 passes, rutting appeared to be similar to that of Repair 3, and trafficking was discontinued to allow the load cart to be used to apply traffic to other repairs.

Table 17. Repair 4 rut depth data.

Pass # — TOTAL	Maximum Rut Depth (in.)		
	East[a]	Center[a]	West[a]
0	0.24	0.84	0.48
10	0.36	0.84	0.72
20	0.36	0.84	0.72
30	0.60	0.84	0.72
50	0.60	0.84	0.72
80	0.60	0.84	0.72
100	0.60	0.84	0.72

[a] East, center, and west refer to the data collection locations across the repair.

Table 18 displays rut depth data at several pass levels for Repair 5, which was backfilled with sand-filled geocell and capped with FRP. As shown, the failure criterion of 3 in. was not exceeded until 175 passes had been reached. The data agree reasonably well with similar results found in

Garcia et al. (2021), where approximately 2.75 in. of rutting was measured at 175 passes for the same geocell backfilled with an SP material.

Table 18. Repair 5 rut depth data.

Pass # — TOTAL	Maximum Rut Depth (in.)		
	East[a]	Center[a]	West[a]
0	0.12	0.12	0.12
10	1.08	1.20	1.44
20	1.92	1.92	1.92
30	2.04	2.28	2.16
75	2.76	2.28	2.16
100	2.76	2.64	2.40
130	3.00	2.76	2.40
150	3.00	3.00	2.64
175	3.12	3.12	2.76

[a] East, center, and west refer to the data collection locations across the repair.

Table 19 shows the rut depth data for Repair 6. Trafficking was discontinued after 500 passes, with very little rutting observed (less than 0.5 in. caused by traffic). No damage to the FRP matting was observed. The surface of the RSFF after the FRP was removed is shown in Figure 60.

Table 19. Repair 6 rut depth data.

Pass # — TOTAL	Maximum Rut Depth (in.)		
	East[a]	Center[a]	West[a]
0	0.36	0.36	0.36
30	0.36	0.48	0.48
100	0.36	0.60	0.48
200	0.36	0.60	0.48
300	0.36	0.60	0.60
400	0.48	0.72	0.84
500	0.48	0.84	0.60
[b]Forensic	0.36	0.60	0.60

[a] East, center, and west refer to the data collection locations across the repair.

[b] Rut measurement conducted after FRP removal during forensic evaluation.

Figure 60. Repair 6, overall surface of RSFF backfill, 500 passes.

Repair 7 was backfilled with dry-placed RSFF and capped with RSC. The RSC appeared to reach initial set after approximately 12 hr of curing (Figure 61), and trafficking commenced after 18 hr of curing. Some small shrinkage cracks appeared before trafficking, but they did not propagate during trafficking (Figure 62). Table 20 contains the rut depth data for Repair 7. Trafficking continued until 1,000 passes had been applied with virtually zero deformation observed overall during trafficking.

Figure 61. Repair 7, 12 hr cure time, 0 passes.

Figure 62. Small shrinkage cracking on Repair 7, 18 hr cure time, 0 passes.

Figure 63. Repair 7, overall, 1,000 passes.

Table 20. Repair 7 rut depth data.

Pass # — TOTAL	Maximum Rut Depth (in.)		
	East[a]	Center[a]	West[a]
0	0.24	0.36	0.48
30	0.36	0.48	0.48
100	0.36	0.48	0.48
200	0.36	0.48	0.48
300	0.36	0.48	0.48
400	0.36	0.48	0.48
500	0.36	0.48	0.48
750	0.36	0.48	0.36
1000	0.36	0.48	0.48

[a] East, center, and west refer to the data collection locations across the repair.

5.3 Additional Characterization Data

In addition to the trafficking data collection described in the previous section, additional types of data were collected to further characterize the repairs. The RSP and DCP were used to track penetration resistance of the compacted snow and ice, and the heavy weight deflectometer (HWD) was used to estimate impulse-stiff modulus (ISM) over time of several repairs. These data are provided along with analysis in the following sections.

5.3.1 Penetrometer Test Results

Figure 64 and Figure 65 show the DCP and RSP strength changes, respectively, over time for three defined layers in the snow backfill of Repair 2 - Layer 1: 25–125 mm; Layer 2: 125–275 mm; and Layer 3: 275–400 mm. Despite not having many opportunities for snow measurements at Repair 2 (owing to the FRP cover in place), RSP strength gain was slow and minimal over the first 50 hr after construction. Strength gains were significant between 50 and 68 hr compared to the time between about 10 and 50 hr. This change in strengthening rate was likely associated with the removal of the FRP for a day to allow maintenance to a limited area that displayed excessive rutting. Snow sintering (natural metamorphic bonding between ice particles) would have been greatly impeded by the FRP cover blocking vapor transport between the snow mass and the air.

Figure 64. DCP strength index history for Repair 2.

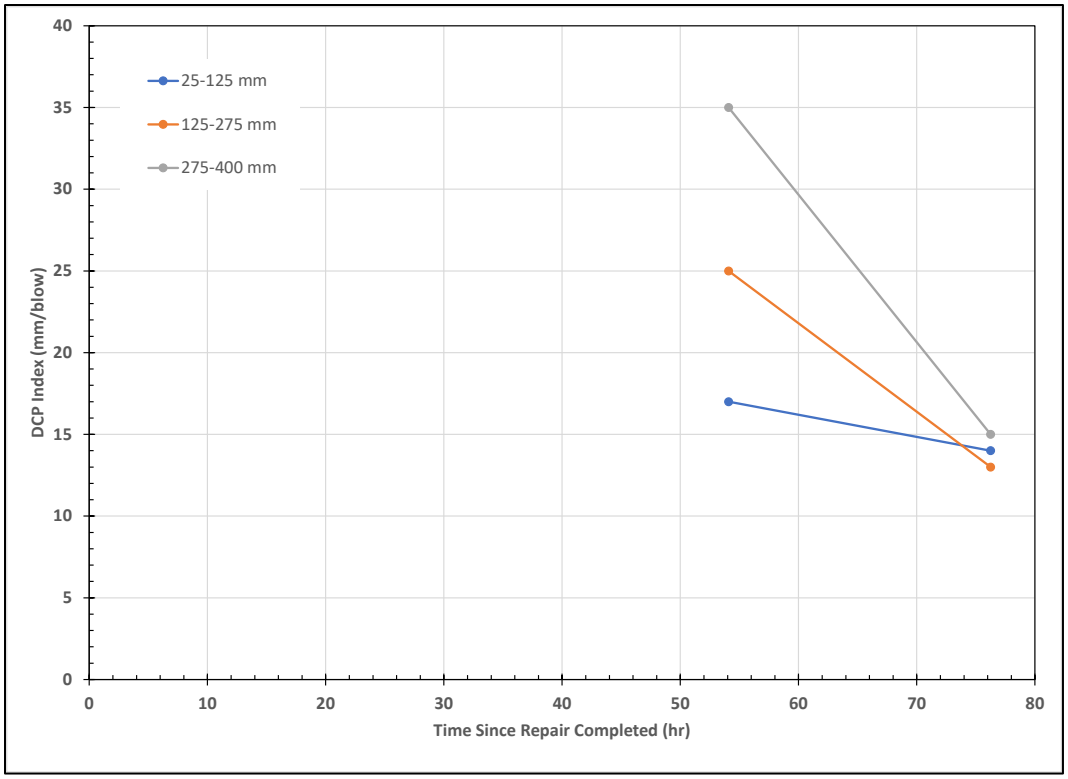

Figure 65. RSP strength index history for Repair 2.

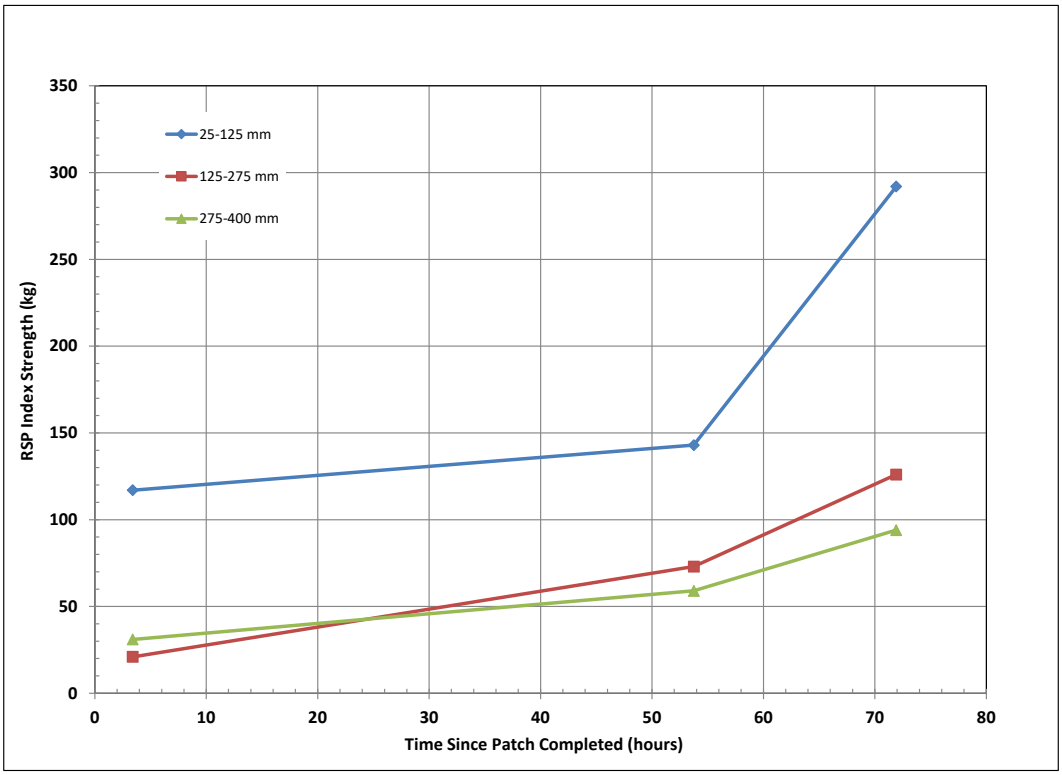

DCP and RSP strength characterization for the three defined layers in the snow backfill of Repair 3 is shown in Figure 66 and Figure 67, respectively. Initial RSP strengths in Repair 3 are similar to those observed in Repair 2. Repair 3 strength gains were significant over the first 24 hr, then oddly fell over the next 24 to 48 hr period before again rising. Still, the Repair 3 RSP strength at the 48 hr point was greater than that seen in Repair 2 at the same time. This more rapid strengthening in Repair 3 compared to Repair 2 was associated with Repair 3's being continuously open to the atmosphere during curing.

Despite the unexpected decrease and then recovery of strength as recorded by the RSP between 24 and 72 hr, the DCP showed identical behavior. This suggests that the data are not in error. However, it is still plausible that the loss and recovery of strength is an indication of anisotropy in the snow mass, rather than an actual reduction in strengthening over time.

Interestingly, despite the retardation of strengthening caused by the FRP cover on Repair 2, by the 72 hr time interval, Repair 2 showed similar strength levels to Repair 3 in both RSP and DCP measurements.

Figure 66. DCP strength index history for Repair 3.

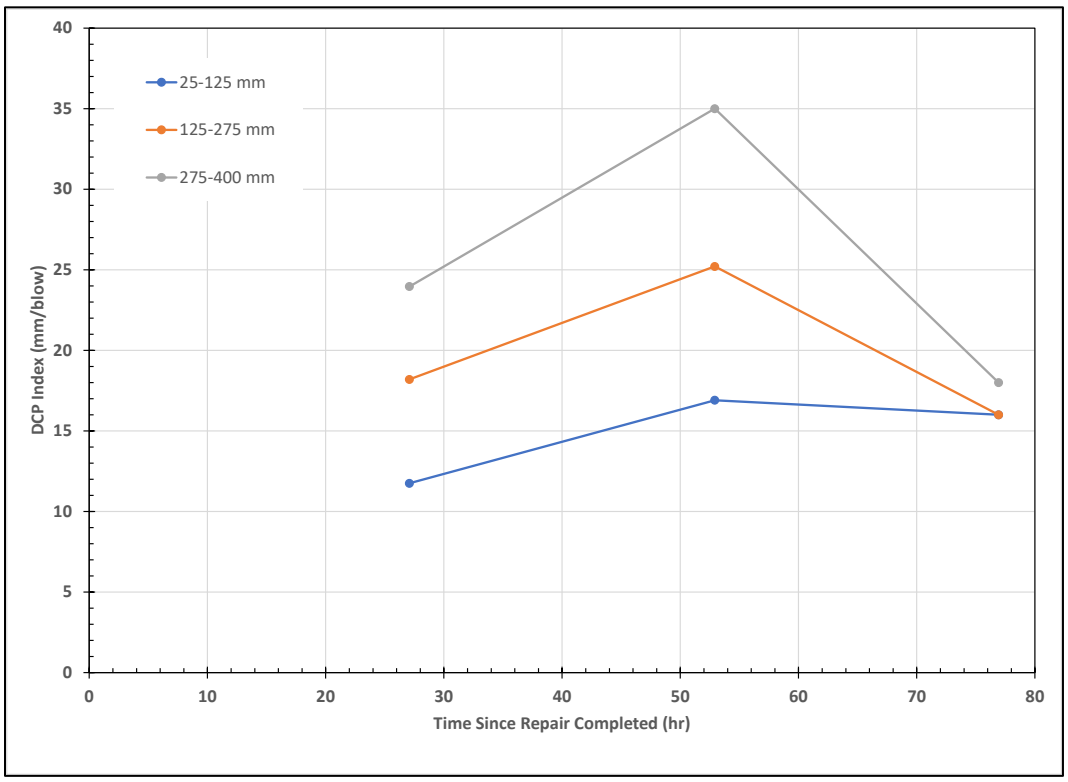

Figure 67. RSP strength index history for Repair 3.

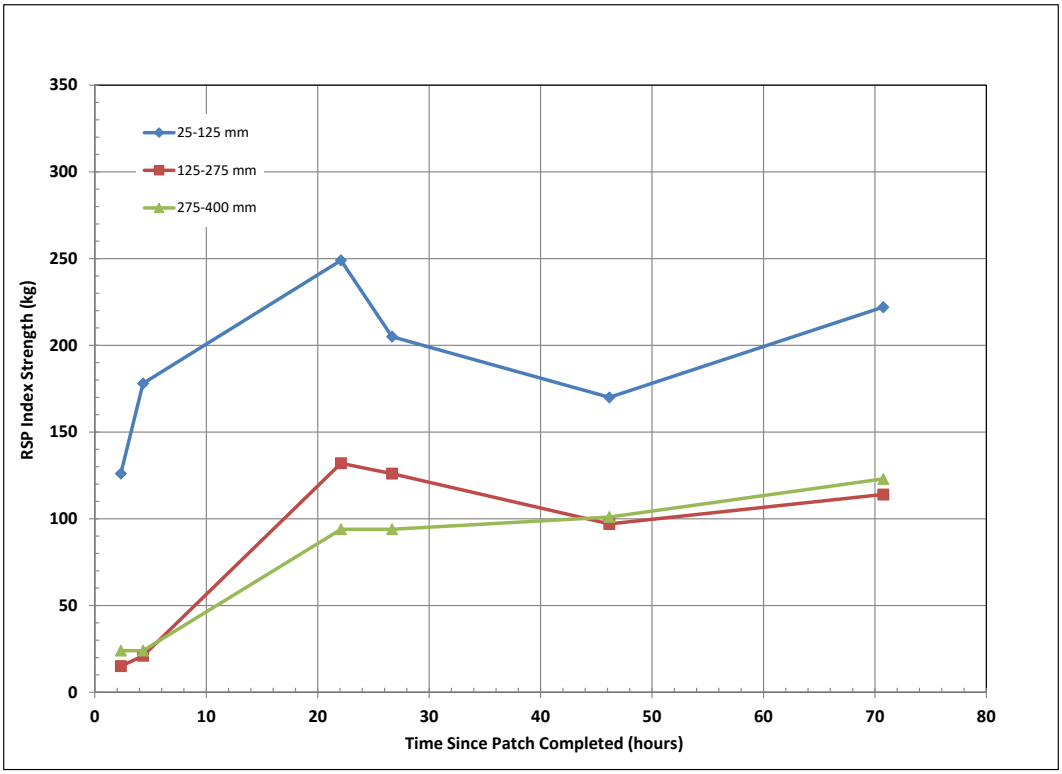

Penetrometer measurements (DCP and RSP) were again used to track index strength changes with time after Repair 4 was completed (Figure 68 and Figure 69). These tests were conducted side by side, as was done for Repair 3. Initial RSP strengths in Repair 4 were slightly less than, but similar to, the strengths observed in Repairs 2 and 3 for Layers 2 and 3. Layer 1's strength in Repair 4 shortly after repair completion was considerably less than what was seen in Repairs 2 and 3.

Twenty-four hours after patch completion, Repair 4's Layers 1 and 2 RSP strengths were like those measured in Repair 3; Layer 3 significantly lagged in strength development. Two layers show a dip in RSP strength between hours 22 and 26, but then all layers continue to strengthen. Unlike Repairs 2 and 3, the Repair 4 DCP data between 24 and 72 hr did not trend as closely with the RSP measurements. In the DCP data for Repair 4, Layer 3 shows a huge increase in strength during this period, but Layers 1 and 2 show a steady strength level. Some of these differences may again be attributed to variations in snow properties within the areas where side-by-side testing took place and taking measurements at varied locations at different time intervals. Nonetheless, the trends shown by both the DCP and RSP agree.

As was observed in laboratory results (Asenath-Smith et al. 2019) and demonstrated during HWD testing, wetted snow with included cellulose achieves a higher ultimate strength than wetted snow alone but is slower in its rate of strength gain during the first 48 hr of curing. Both DCP (Figure 64 and Figure 66) and RSP (Figure 65 and Figure 67) results support this finding with notably greater strengths at 72 hr in Repair 4 compared to Repair 3. Further, the RSP data (Figure 65 and Figure 67), particularly during the first 18 hr, support our prior conclusion that adding cellulose to wetted snow slows its initial strength gain.

Figure 68. DCP strength index history for Repair 4.

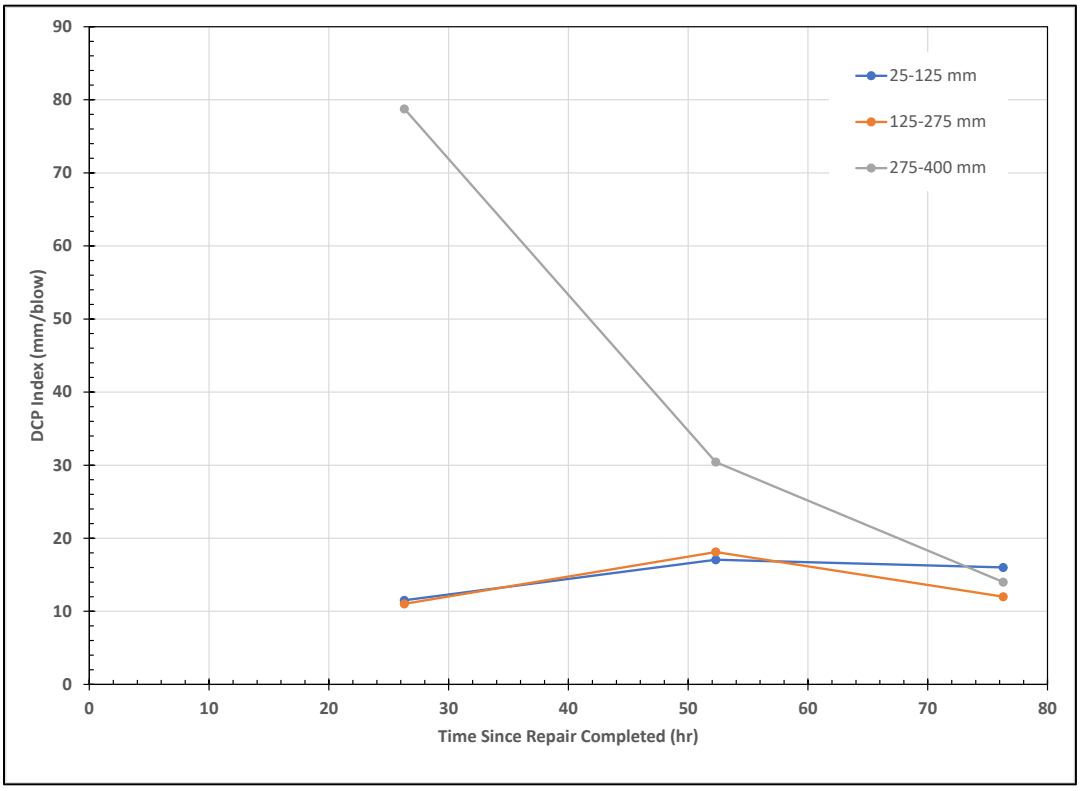

Figure 69. RSP strength index history for Repair 4.

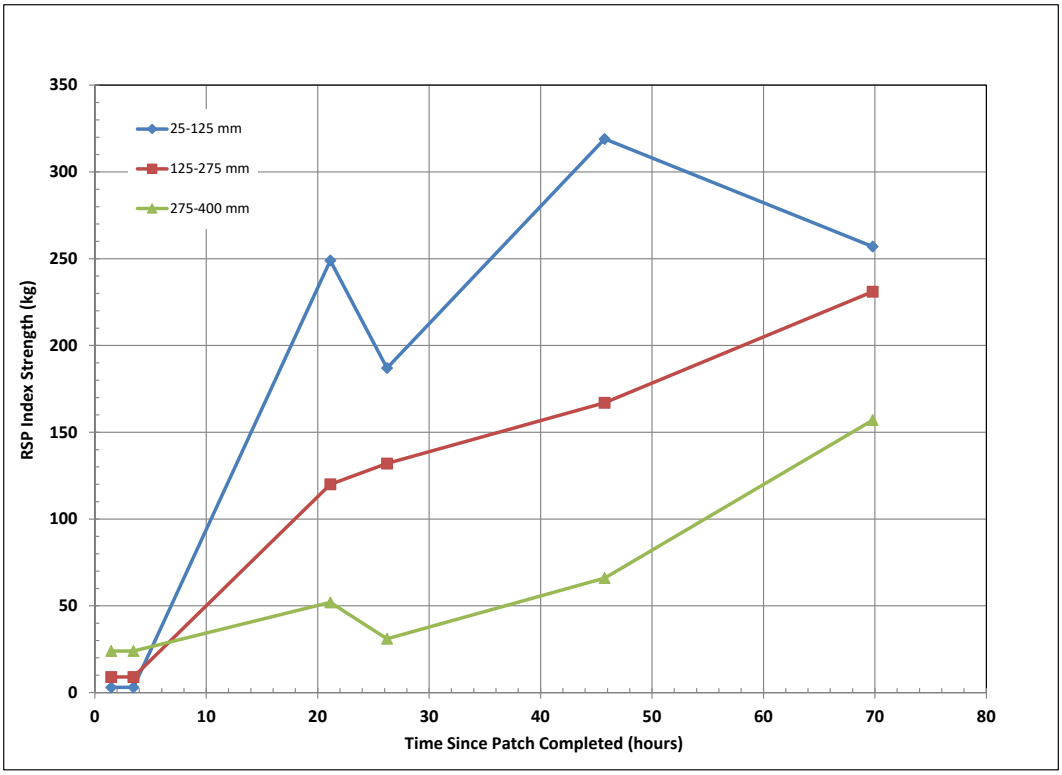

After trafficking, DCP testing was attempted on Repair 6, which was backfilled with RSFF. Three attempts all resulted in refusal of the test device. This result indicates an approximate CBR of 100 or greater of the backfill material.

5.3.2 Snow Density Test Results

In most materials, density is closely linked to strength. While tightly packed ice particles make for a stronger snow, it is the intergranular bonding (ice connectors) between particles that primarily dictates how much load a snow surface can support. The strength of these bonds can vary widely for a given density snow. This is because ice is a strongly metamorphic material in natural settings owing to its proximity to its melting point. Penetrometer measurements represent a combined density and bonding index of snow strength.

A successful snow pavement requires a high level of snow strength which can only be achieved by starting with a closely packed mass of ice particles. Obviously, a dense snow resists deformation due to the high force needed to either further decrease porosity or cause grains to displace relative to each other. Additionally, high-density snow has many intergranular

contact points where bonds can develop and lock grains together. Environmental factors like temperature, solar exposure, and wind (but not rain or water infiltration) only slowly cause natural changes in density (on a scale of weeks) in contrast to bond strength, which can change notably over the course of only 24 hr.

Density measurements were obtained by drilling cores samples from Repairs 3 and 4 (Figure 70), sectioning the ice cylinder (Figure 71), and dividing each piece's weight by its volume. During this process, the core was observed for layering, contaminates, or other potential weak points. Excellent uniformity was observed in all the cores we obtained; no evidence could be seen of the boundary between construction layers.

Figure 70. Core drilling compacted snow-water slurry sample.

Figure 71. Core sectioning for weight and volume measurement to calculate density.

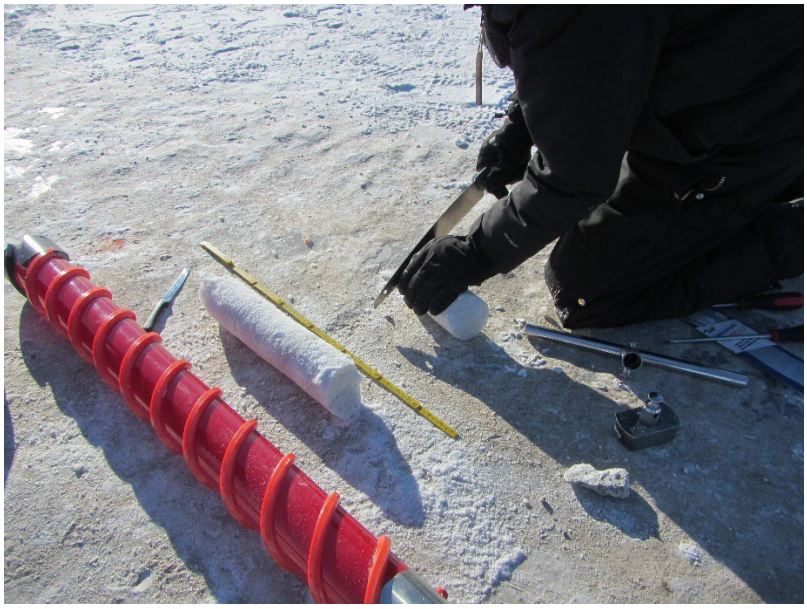

Density values for Repairs 3 and 4 are shown in Table 21. Repair 2 was covered and inaccessible when sampling was performed, but, owing to similar construction techniques, it would be expected to yield similar densities to Repairs 3 and 4. As discussed earlier, each layer (horizon) in a snow pavement plays a role in the support of aircraft loads. While we have established that for each aircraft type a different penetrometer level represents the lower strength limit for each layer to assure the snow pavement fully supports the aircraft landing gear, the same is not true for density. Our experience with airfield snow pavement construction indicates that a density over 0.6 g/cm^3 (40% porosity or 0.6 specific gravity) is necessary throughout at least the top meter of snowpack for it to achieve (through bond formation) an adequate level of strength to support heavy wheel loads and contact pressures. Both Repairs 3 and 4 met this minimum density target, with the wetted, cellulose-included snow (Repair 4) having a slightly higher average density 0.71 g/cm^3 than the wetted snow alone (Repair 3) at 0.67 g/cm^3.

Table 21. Compacted snow water slurry density results.

Repair 3		Repair 4	
Layer (cm)	Density (g/cm^3)	Layer (cm)	Density (g/cm^3)
0–11	0.69	0.5–5.5	0.75
12–25	0.66	7–20	0.67

5.3.3 Heavy-Weight Deflectometer Results

The overall stiffness of each repair was evaluated using the HWD, as shown in Figure 72. The force measured from the load cell was divided by the deflection measured directly under the plate (D1) to calculate the ISM. ISM was measured periodically to assess stiffness gain during curing and stiffness reduction during trafficking. In many cases, when HWD testing was attempted, the deflection reached a level that overranged the sensor, which prevented an ISM from being measured. All ISMs collected successfully are shown in Table 22 and further discussed in the following paragraphs.

Figure 72. Heavy weight deflectometer (HWD) test device.

Table 22. ISM results from HWD testing.

Repair #	Cure Time (hr)	ISM (kips/in.)
1	24	—[a]
1	40	1509
1	48	587
1	96	917
1	108	1871
2	4	—[a]
2	24	655
2	48	—[a]
2	120	—[a]
3	4	317
3	24	1,557
3	48	1,690
3	120	1,373
4	4	—[a]
4	24	804
4	48	1,006
4	120	1,321
L3[b]	40	714[b]
L4[b]	24	2,910[b]
L4[b]	40	2,230[b]
Parent Slab[c]	—	6,228[c]

[a] Sensors overranged when HWD testing was attempted.

[b] ISM was measured after 500 simulated aircraft passes.

[c] Test was conducted on existing concrete before any repairs.

HWD results for Repair 1 are displayed graphically in Figure 73. The ISM was initially approximately 1,500 kips/in. before dropping substantially over the next few days. However, at 108 hr, the ISM recovered to surpass the initial ISM. Repair 1 was completed at 1,700 on 21 January; and, as shown in Appendix A, several large temperature swings occurred during the curing period (wind chills ranged from −22°F to 19°F), which could have affected the strength development of the ice as well as the HWD test results. Overall, these results indicate that the water-filled debris method could be adequate to withstand aircraft loading structurally, but because it was not trafficked, the near surface capacity is unknown.

Figure 73. Repair 1 impulse-stiffness modulus (ISMs).

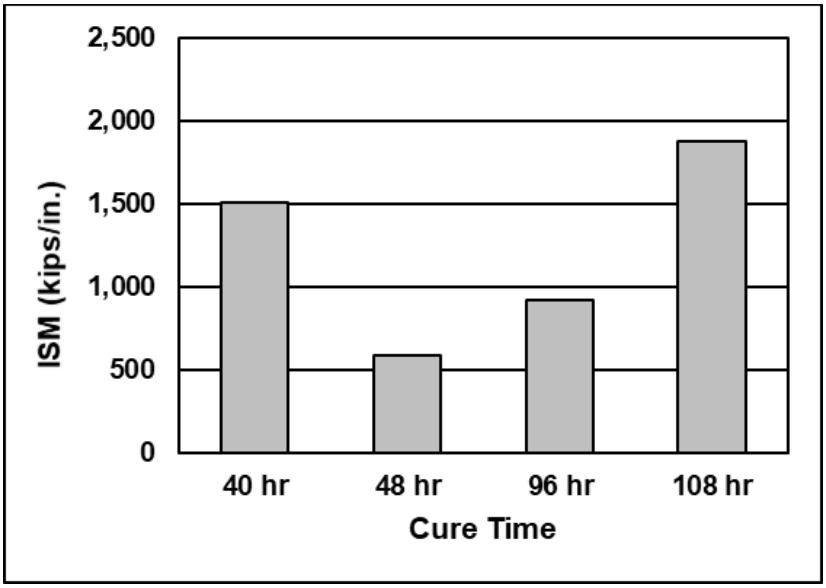

ISMs for Repairs 3 and 4 are shown in Figure 74. The ISM for Repair 3 was nearly twice that of Repair 4 after 24 hr of cure time. At 48 hr of cure time, ISMs for both repairs increased slightly. After 500 passes were applied (cure time 120 hr), the ISMs were nearly identical with Repair 3's decreasing slightly under traffic while Repair 4's increased compared to the 48 hr cure time. These results suggest that the cellulose fibers used in Repair 4 could have required an increased cure time while adding the benefit of increased durability under traffic.

Figure 74. Repairs 3 and 4 ISMs.

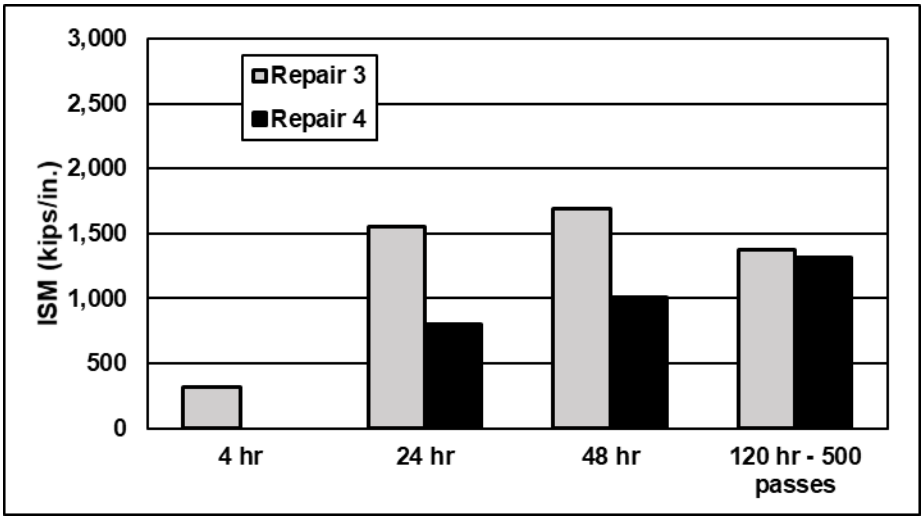

Figure 75 shows ISM levels of Repairs 6 and 7 at various pass levels and cure times. The ISM of Repair 6 was able to be measured only at the end of

trafficking after removal of the FRP mat (500 passes and 24 hr cure time). Repair 7's ISM was measured at the beginning of traffic (after 18 hr of curing) and twice at a traffic level of 500 passes (24 hr and 40 hr cure). As expected, the ISM level of Repair 6 was much lower than that of Repair 7, since it was tested on an RSFF surface as opposed to an RSC surface. Still, an ISM of over 700 kips/in. indicated a considerably stiff repair comparable to that of low-quality concrete repairs as discussed in Bell et al. (2022). As expected, the ISM dropped slightly after 500 aircraft passes at the 24 hr cure time and then slightly increased at the 40 hr cure time.

Figure 75. Repair 6 and 7 ISMs.

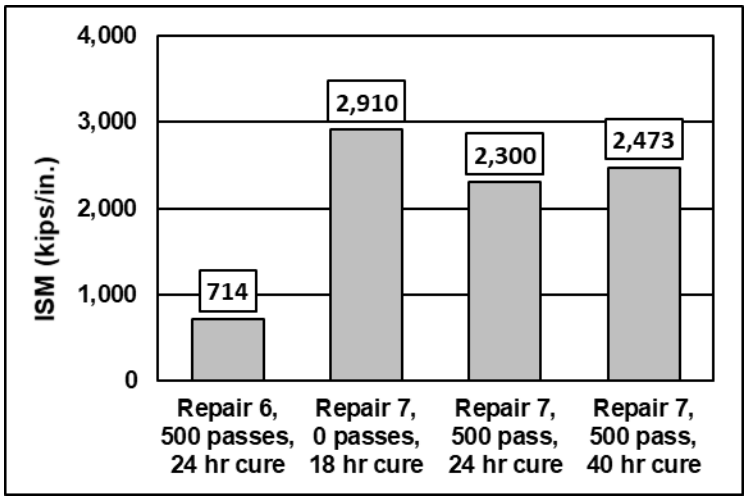

6 Conclusions and Recommendations

6.1 Conclusions

The laboratory testing and full-scale experiment described in this report developed the following overall conclusions:

- Laboratory-scale testing indicated that the CARTS system provided a realistic curing environment for investigating RSC properties at extremely low temperatures.

- Laboratory-scale testing indicated that when heated water was used, RSC could be a viable option for capping repairs down to 10°F.

- Mechanical functionality of the equipment did not appear to be affected substantially by the extremely cold temperatures. Some issues occurred but were not directly attributed to temperature.

- For the marking task, lumber crayons were effective for marking in lieu of spray paint, which can be difficult to use in extremely cold temperatures.

- Pavement cutting times were much slower than those recorded in previous troop demonstrations. The CTL tracks were slipping considerably during cutting due to the presence of a sheet of ice approximately 1 in. thick on the surrounding pavement. However, cutting was still accomplished by making a series of two to three plunges of the saw on each side of the repair.

- Repairs backfilled with compacted snow and ice (allowed to freeze for 48 hr) were completed successfully and able to withstand 500 passes of simulated C-17 traffic without any notable distresses.

- Use of cellulose additive with compacted snow and ice repairs did not appear to greatly affect the rutting performance of the repair but increased overall stiffness. Freezing time also increased slightly due to cellulose addition.

- RSFF as a backfill for FRP exhibited excellent performance, sustaining 500 passes of simulated C-17 traffic with no distresses. RSFF also

appeared to perform as it does in temperate climates as a backfill for RSC. The only difference observed was a slight increase in percolation time possibly due to initial freezing of some of the mix water.

- RSC took substantially longer to cure (12 hr) in extremely cold temperatures but performed well under trafficking, exhibiting very little distress after 1,000 passes of simulated C-17 traffic.

6.2 Recommendations

After considering the specific test results, analysis, and the conclusions discussed in the previous sections, the following specific recommendations were developed:

- Existing RADR solutions should be considered suitable in extremely cold temperatures (down to approximately 0°F), with the following minor modifications:
    - The pavement immediately adjacent to the repair should be fully cleared of any snow or ice (as much as possible) to reduce CTL track slippage during pavement cutting so that the time required to cut does not increase considerably.
    - The SVM should be modified to include electrically powered heat tape wrapped around the water supply lines, water pump, pressure washer supply lines, and pressure washer pump to prevent freezing.
    - When possible, heated water (approximately 70°F) should be used for RSFF and RSC. Heated water should allow faster percolation for RSFF and decreased set times for RSC.
    - All equipment should be properly prepared for operation in extremely cold temperatures (down to approximately 0°F). Most RADR equipment is available commercially as off-the-shelf items, so consulting with the manufacturer for proper cold weather preparation procedures is recommended.
- The compacted snow and ice backfill method should be considered as a suitable approach for backfilling crater repairs in very cold

temperatures (approximately 0°F) when higher quality materials are unavailable.

- We recommend further investigation to refine freezing times for compacted snow and ice backfill in a wide range of temperatures.

- We recommend further investigation to develop improved TTPs for placing RSC at temperatures near 0°F. Only one repair was able to be conducted for this investigation, so variations of material and water temperature for a full-scale repair operation could not be fully investigated. While the repair conducted performed well under traffic, cure time was increased considerably above the target for RADR operations.

- We recommend a market survey to identify mobile equipment capable of heating large quantities of RSFF and RSC mix water.

- We recommend future full-scale troop demonstrations with the full RADR major repair kit incorporating solutions identified from the additional investigations recommended previously in this section.

References

Asenath-Smith, E., T. D. Melendy, A. M. Menke, A. P. Bernier, and G. L. Blaisdell. 2019. *Evaluation of Airfield Damage Repair Methods for Extreme Cold Temperatures*. ERDC/CRREL TR-19-2. Vicksburg, MS: US Army Engineer Research and Development Center, Cold Regions Research and Engineering Lab. https://hdl.handle.net/11681/32298.

ASTM (American Society for Testing and Materials). 2015. *Standard Test Method for Compressive Strength of Concrete Cylinders Cast in Place in Cylindrical Molds*. C873. West Conshohocken, PA: ASTM International. https://www.astm.org/c0873_c0873m-15.html.

ASTM (American Society for Testing and Materials). 2017a. *Standard Practice for Classification of Soils for Engineering Purposes (Unified Soil Classification System)*. D2487. West Conshohocken, PA: ASTM International. https://www.astm.org/d2487-17.html.

ASTM (American Society for Testing and Materials). 2017b. *Standard Test Method for Flow Consistency of Controlled Low Strength Material (CLSM)*. D6103. West Conshohocken, PA: ASTM International.

ASTM (American Society for Testing and Materials). 2018. *Standard Test Method for Use of Dynamic Cone Penetrometer in Shallow Pavement Applications*. D6951. West Conshohocken, PA: ASTM International.

ASTM (American Society for Testing and Materials). 2021. *Standard Test Method for Compressive Strength of Cylindrical Concrete Specimens*. Designation: C39. West Conshohocken, PA: ASTM International. https://www.astm.org/c0039_c0039m-21.html.

Bell, H. P. 2017. *Inclement Weather Crater Repair Tool Kit*. ERDC/GSL TR-17-26. Vicksburg, MS: US Army Engineer Research and Development Center, Geotechnical and Structures Lab. http://hdl.handle.net/11681/25667.

Bell, H. P., W. D. Carruth, J. L. Daugherty, L. Garcia, A. B. Ward, W. C. Floyd, L. Edwards, J. S. Tingle, J. R. Davis, Jr., J. F. Rowland, C. R. Lloyd, Jr., and T. T. Henderson, Sr. 2022. *Expedient and Expeditionary Airfield Damage Repair (E-ADR) Joint Capability Technology Demonstration (JCTD) Operational Demonstration #1*. ERDC/GSL TR-22-14. Vicksburg, MS: US Army Engineer Research and Development Center.

Bell, H. P., B. C. Cox, L. Edwards, L. I. Garcia, N. R. Hoffman, M. Mejias-Santiago, and J. L. Johnson. 2019. *Rapid Airfield Damage Recovery Technology Integration Experiment*. ERDC/GSL TR-19-8. Vicksburg, MS: US Army Engineer Research and Development Center, Geotechnical and Structures Lab. https://hdl.handle.net/11681/33049.

Bell, H. P., C. L. Dean, and C. A. Rutland. 2018. *Wet Weather Crater Repair Methods for Grooved and Smooth Pavements*. ERDC/GSL TR-18-6. Vicksburg, MS: US Army Engineer Research and Development Center, Geotechnical and Structures Lab. http://hdl.handle.net/11681/27103.

Bell, H. P., L. Edwards, W. D. Carruth, J. S. Tingle, and J. R. Griffin. 2013. *Wet Weather Crater Repair Testing at Silver Flag Exercise Site, Tyndall Air Force Base, Florida*. ERDC/GSL TR-13-42. Vicksburg, MS: US Army Engineer Research and Development Center, Geotechnical and Structures Lab.

Bell, H. P., and J. Rowland. 2017. *Next Generation Airfield Damage Repair: Deployable Saw Technologies*. ERDC/GSL TR-17-29. Vicksburg, MS: US Army Engineer Research and Development Center, Geotechnical and Structures Lab.

Bell, H. P., L. P. Priddy, Q. S. Mason, and C. A. Rutland. 2015. *Concrete Cutting Refinement for Crater Repair*. ERDC/GSL TR-15-29. Vicksburg, MS: US Army Engineer Research and Development Center. http://hdl.handle.net/11681/10470.

Carruth, W. D. 2020. *Laboratory Characterization of Rapid-Setting Flowable Fill*. ERDC/GSL TR-20-11. Vicksburg, MS: US Army Engineer Research and Development Center, Geotechnical and Structures Lab. https://hdl.handle.net/11681/36353.

Carruth, W. D., L. Edwards, H. P. Bell, J. S. Tingle, J. R. Griffin, and C. A. Rutland. 2015. *Large Crater Repair at Silver Flag Exercise Site, Tyndall Air Force Base, Florida*. ERDC/GSL TR-15-27. Vicksburg, MS: US Army Engineer Research and Development Center, Geotechnical and Structures Lab. http://hdl.handle.net/11681/10472.

Carruth, W. D., and I. L. Howard. 2016. *Evaluation of Flowable Fill Surface Performance*. ERDC/GSL TR-16-33. Vicksburg, MS: US Army Engineer Research and Development Center, Geotechnical and Structures Lab. http://hdl.handle.net/11681/20423.

Departments of the Army, Navy, and Air Force. 2003. *Airfield Damage Repair*. Unified Facilities Criteria UFC 3-270-07. Washington, DC: Headquarters, Departments of the Army, Navy, and Air Force.

Edwards, L., H. P. Bell, W. D. Carruth, J. R. Griffin, and J. S. Tingle. 2013. *Cold Weather Crater Repair Testing at Malmstrom Air Force Base, Montana*. ERDC/GSL TR-13-32. Vicksburg, MS: US Army Engineer Research and Development Center, Geotechnical and Structures Lab.

Edwards, L., W. D. Carruth, J. S. Tingle, and I. L. Howard. 2018. *Rapid Setting Flowable Fill Performance in Cold Weather for Airfield Damage Repair*. ERDC/GSL TR-18-26. Vicksburg, MS: US Army Engineer Research and Development Center. http://hdl.handle.net/11681/29531.

Garcia, L., J. Rowland, and J. S. Tingle. 2021. *Evaluation of Geocell-Reinforced Backfill for Airfield Pavement Repair*. ERDC/GSL TR-21-41. Vicksburg, MS: US Army Engineer Research and Development Center. https://hdl.handle.net/11681/42550.

Gartrell, C. A. 2007. *Investigations for Airfield Damage Repair Kit Modifications and Improvements*. ERDC/GSL TR-07-16. Vicksburg, MS: US Army Engineer Research and Development Center, Geotechnical and Structures Lab.

Gartrell, C. A. 2008. *Investigations for Airfield Damage Repair Kit Modifications and Improvements, Phase II*. ERDC/GSL TR-08-09. Vicksburg, MS: US Army Engineer Research and Development Center.

Haehnel, R. B., G. L. Blaisdell, T. Melendy, S. Shoop, and Z. Courville. 2019. *A Snow Runway for Supporting Wheeled Aircraft: Phoenix Airfield, McMurdo, Antarctica*. ERDC/CRREL TR-19-4. Vicksburg, MS: US Army Engineer Research and Development Center, Cold Regions Research and Engineering Lab. https://hdl.handle.net/11681/32731.

Johnson, T. R., C. A. Weiss, L. Edwards, J. S. Tingle, W. S. Harmon, and T. J. Talbot. 2018. *Laboratory Evaluation of Next-Generation Backfill Materials and Methods for Airfield Damage Repair*. ERDC/GSL TR-18-33. Vicksburg, MS: US Army Engineer Research and Development Center, Geotechnical and Structures Lab. http://hdl.handle.net/11681/31445.

Mann, T. A., R. B. Freeman, and G. L. Anderton. 2007. *Grout Impregnation of Pre-Placed Recycled Concrete Pavement (RCP) for Rapid Repair of Deteriorated Portland Cement Concrete Airfield Pavements*. ERDC/GSL TR-07-9. Vicksburg, MS: US Army Engineer Research and Development Center, Geotechnical and Structures Lab. http://hdl.handle.net/11681/10573.

Mejias-Santiago, M., J. L. Johnson, L. A. Gurtowski, C. S. Griggs, and C. A. Rutland. 2017. *Refinement of Foam Backfill Technology for Expedient Airfield Damage Repair. Phase II, Development of Prototype Foam Dispensing Equipment and Improved Tactics, Techniques, and Procedures*. ERDC TR-17-4. Vicksburg, MS: US Army Engineer Research and Development Center. http://hdl.handle.net/11681/25903.

Mejias-Santiago, M., B. Ruiz-Cruz, L. A. Gurtowski, C. S. Griggs, J. L. Johnson, and D. R. Felt. 2016. *Refinement of Foam Backfill Technology for Expedient Airfield Damage Repair; Phase I: Laboratory Evaluation of Foam Materials*. ERDC TR-16-16. Vicksburg, MS: US Army Engineer Research and Development Center. http://hdl.handle.net/11681/20414.

Oren, J. I., R. D. Moser, V. Boddu, C. A. Weiss Jr, and J. Clausen. 2014. *Laboratory Evaluation of Expedient Low-Temperature Admixtures for Runway Craters in Cold Weather*. ERDC/GSL TR-14-10. Vicksburg, MS: US Army Engineer Research and Development Center, Geotechnical and Structures Lab. http://hdl.handle.net/11681/8562.

Priddy, L. P., H. P. Bell, L. Edwards, W. D. Carruth, and J. F. Rowland. 2016. *Evaluation of the Structural Performance of Rapid Set Concrete Mix®*. ERDC/GSL TR-16-20. Vicksburg, MS: US Army Engineer Research and Development Center. https://apps.dtic.mil/sti/citations/AD1013578.

Priddy, L. P., J. R. Griffin, and J. S. Tingle. 2011a. *Live-flight Certification Testing of CRATR Technologies, Avon Park Air Force Range, Florida*. ERDC/GSL TR 11-7. Vicksburg, MS: US Army Engineer Research and Development Center, Geotechnical and Structures Lab.

Priddy, L. P., T. W. Rushing, and J. S. Tingle. 2011b. *Live-Flight Certification Testing of Deployable Crater Repair Technologies, Avon Park Air Force Range, Florida*. ERDC/GSL TR 11-1. Vicksburg, MS: US Army Engineer Research and Development Center, Geotechnical and Structures Lab.

Priddy, L. P., J. S. Tingle, M. C. Edwards, J. R. Griffin, and T. J. McCaffrey. 2013a. *Critical Runway Assessment and Repair (CRATR) Technology Demonstration: Limited Operational Utility Assessment 2 (LOUA2), Tyndall Air Force Base, Florida*. ERDC/GSL TR-13-39. Vicksburg, MS: US Army Engineer Research and Development Center, Geotechnical and Structures Lab.

Priddy, L. P., J. S. Tingle, J. R. Griffin, M. C. Edwards, and T. J. McCaffrey. 2013b. *Critical Runway AssessmenT and Repair (CRATR) Technology Demonstration: Operational Utility Assessment (OUA), Avon Park Air Force Range, Florida*. ERDC/GSL TR-13-33. Vicksburg, MS: US Army Engineer Research and Development Center.

Rushing, J. F., W. C. Floyd, D. E. Harder, T. W. Rushing, W. D. Carruth, G. E. Johnston, and J. C. Ray. 2016a. *Evaluation of the Army Light Airfield Repair Package (LARP) Contents*. ERDC/GSL TR-16-32. Vicksburg, MS: US Army Engineer Research and Development Center.

Rushing, J. F., W. C. Floyd, T. W. Rushing, L. Garcia, W. D. Carruth, J. S. Tingle, and C. A. Rutland. 2016b. *Validation of FRP Matting Requirements*. ERDC/GSL TR-16-22. Vicksburg, MS: US Army Engineer Research and Development Center, Geotechnical and Structures Lab. http://hdl.handle.net/11681/20349.

Tingle, J. S., L. P. Priddy, M. C. Edwards, C. A. Gartrell, and T. J. McCaffrey. 2009. *Critical Runway Assessment and Repair (CRATR) Technology Demonstration: Limited Operational Utility Assessment 1 (LOUA1), Tyndall Air Force Base, Florida*. ERDC/GSL TR-09-12. Vicksburg, MS: US Army Engineer Research and Development Center, Geotechnical and Structures Lab.

USAF (United States Air Force). 1992. *Crushed-Stone Crater Repair and Line-of-Sight Profile Measurement for Rapid Runway Repair*. T.O. 35E2-5-1. Washington, DC: US Air Force.

Appendix A: Hourly Weather Data

Table A-1. Hourly weather data 15 January 2020.

Time	Temperature (°F)	Wind Speed (mph)	Wind Chill (°F)	Condition
1:00 AM	–4	10	–21	Fair
2:00 AM	–6	9	–22	Fair
3:00 AM	–9	10	–27	Mostly Cloudy
4:00 AM	–9	7	–24	Partly Cloudy
5:00 AM	–8	10	–26	Fair
6:00 AM	–9	2	–14	Fair
7:00 AM	–8	3	–16	Mostly Cloudy
8:00 AM	–8	0	–8	Mostly Cloudy
9:00 AM	–8	8	–24	Mostly Cloudy
10:00 AM	–6	13	–26	Cloudy
11:00 AM	–4	8	–19	Cloudy
12:00 PM	0	9	–15	Mostly Cloudy
1:00 PM	3	8	–10	Mostly Cloudy
2:00 PM	5	8	–8	Mostly Cloudy
3:00 PM	7	10	–7	Partly Cloudy
4:00 PM	9	9	–4	Mostly Cloudy
5:00 PM	9	8	–3	Mostly Cloudy
6:00 PM	7	5	–2	Mostly Cloudy
7:00 PM	3	9	–11	Mostly Cloudy
8:00 PM	5	9	–9	Fair
9:00 PM	1	12	–16	Fair
10:00 PM	1	9	–14	Fair
11:00 PM	–4	7	–18	Fair
12:00 AM	–6	7	–20	Fair

Table A-2. Hourly weather data 16 January 2020.

Time	Temperature (°F)	Wind Speed (mph)	Wind Chill (°F)	Condition
1:00 AM	–6	8	–21	Fair
2:00 AM	–4	9	–20	Fair
3:00 AM	–8	12	–28	Fair
4:00 AM	–9	3	–17	Fair
5:00 AM	–11	8	–28	Fair
6:00 AM	–11	9	–29	Fair
7:00 AM	–13	6	–27	Mostly Cloudy
8:00 AM	–11	7	–26	Mostly Cloudy
9:00 AM	–11	10	–30	Mostly Cloudy
10:00 AM	–9	5	–21	Mostly Cloudy
11:00 AM	–6	9	–22	Mostly Cloudy
12:00 PM	–2	14	–21	Mostly Cloudy
1:00 PM	0	16	–20	Mostly Cloudy
2:00 PM	1	15	–18	Mostly Cloudy
3:00 PM	1	15	–18	Fair
4:00 PM	3	16	–16	Fair
5:00 PM	1	10	–15	Fair
6:00 PM	0	9	–15	Fair
7:00 PM	0	6	–12	Fair
8:00 PM	–2	12	–20	Fair
9:00 PM	–6	9	–22	Fair
10:00 PM	–8	8	–24	Fair
11:00 PM	–8	8	–24	Fair
12:00 AM	–9	10	–27	Fair

Table A-3. Hourly weather data 17 January 2020.

Time	Temperature (°F)	Wind Speed (mph)	Wind Chill (°F)	Condition
1:00 AM	−11	8	−28	Fair
2:00 AM	−13	12	−34	Fair
3:00 AM	−13	15	−36	Fair
4:00 AM	−13	21	−40	Fair/Windy
5:00 AM	−15	14	−38	Fair
6:00 AM	−17	7	−34	Fair
7:00 AM	−18	3	−27	Fair
8:00 AM	−17	9	−36	Fair
9:00 AM	−17	7	−34	Fair
10:00 AM	−18	8	−36	Fair
11:00 AM	−15	14	−38	Fair
12:00 PM	−11	8	−28	Fair
1:00 PM	−9	12	−29	Fair
2:00 PM	−9	21	−34	Fair/Windy
3:00 PM	−8	9	−25	Fair
4:00 PM	−8	8	−24	Fair
5:00 PM	−9	3	−17	Fair
6:00 PM	−11	7	−26	Fair
7:00 PM	−11	8	−28	Fair
8:00 PM	−13	7	−29	Fair
9:00 PM	−13	8	−30	Fair
10:00 PM	−13	12	−34	Fair
11:00 PM	−13	13	−35	Fair
12:00 AM	−11	10	−30	Fair

Table A-4. Hourly weather data 18 January 2020.

Time	Temperature (°F)	Wind Speed (mph)	Wind Chill (°F)	Condition
1:00 AM	–11	18	–35	Fair
2:00 AM	–13	13	–35	Fair
3:00 AM	–15	9	–34	Fair
4:00 AM	–17	7	–34	Fair
5:00 AM	–17	5	–30	Fair
6:00 AM	–20	8	–38	Fair
7:00 AM	–15	10	–35	Fair
8:00 AM	–15	13	–37	Fair
9:00 AM	–13	10	–32	Fair
10:00 AM	–13	12	–34	Fair
11:00 AM	–11	17	–35	Mostly Cloudy
12:00 PM	–8	14	–29	Fair
1:00 PM	–4	12	–22	Fair
2:00 PM	0	17	–21	Fair
3:00 PM	1	16	–19	Fair
4:00 PM	1	20	–21	Fair
5:00 PM	–2	15	–22	Fair
6:00 PM	–2	14	–21	Fair
7:00 PM	–4	17	–26	Fair
8:00 PM	–4	16	–25	Fair
9:00 PM	–4	23	–29	Fair/Windy
10:00 PM	–6	20	–30	Fair
11:00 PM	–6	18	–29	Fair
12:00 AM	–6	25	–32	Fair/Windy

Table A-5. Hourly weather data 19 January 2020.

Time	Temperature (°F)	Wind Speed (mph)	Wind Chill (°F)	Condition
1:00 AM	−6	23	−31	Fair/Windy
2:00 AM	−6	20	−30	Fair
3:00 AM	−8	23	−34	Fair/Windy
4:00 AM	−8	16	−30	Fair
5:00 AM	−8	17	−31	Fair
6:00 AM	−8	15	−30	Fair
7:00 AM	−9	8	−25	Fair
8:00 AM	−9	12	−29	Fair
9:00 AM	−11	14	−33	Fair
10:00 AM	−11	21	−37	Fair/Windy
11:00 AM	−9	25	−36	Fair/Windy
12:00 PM	−6	21	−30	Fair/Windy
1:00 PM	−4	20	−27	Fair
2:00 PM	0	16	−20	Fair
3:00 PM	1	18	−20	Fair
4:00 PM	3	15	−16	Fair
5:00 PM	1	9	−14	Fair
6:00 PM	−2	10	−18	Fair
7:00 PM	−4	14	−24	Fair
8:00 PM	−6	3	−14	Fair
9:00 PM	−8	5	−20	Fair
10:00 PM	−13	6	−27	Fair
11:00 PM	−13	2	−18	Fair
12:00 AM	−15	5	−28	Fair

Table A-6. Hourly weather data 20 January 2020.

Time	Temperature (°F)	Wind Speed (mph)	Wind Chill (°F)	Condition
1:00 AM	–15	6	–30	Fair
2:00 AM	–13	10	–32	Fair
3:00 AM	–15	7	–31	Fair
4:00 AM	–15	7	–31	Fair
5:00 AM	–17	10	–37	Fair
6:00 AM	–17	6	–32	Fair
7:00 AM	–18	5	–32	Fair
8:00 AM	–17	5	–30	Fair
9:00 AM	–18	8	–36	Fair
10:00 AM	–15	6	–30	Fair
11:00 AM	–9	2	–14	Fair
12:00 PM	–6	16	–28	Fair
1:00 PM	–4	16	–25	Fair
2:00 PM	–2	18	–24	Fair
3:00 PM	0	15	–19	Fair
4:00 PM	0	15	–19	Fair
5:00 PM	0	14	–19	Fair
6:00 PM	–2	9	–18	Fair
7:00 PM	–2	12	–20	Fair
8:00 PM	–2	9	–18	Mostly Cloudy
9:00 PM	–2	10	–18	Mostly Cloudy
10:00 PM	0	14	–19	Mostly Cloudy
11:00 PM	0	14	–19	Mostly Cloudy
12:00 AM	–2	12	–20	Mostly Cloudy

Table A-7. Hourly weather data 21 January 2020.

Time	Temperature (°F)	Wind Speed (mph)	Wind Chill (°F)	Condition
1:00 AM	–4	8	–19	Mostly Cloudy
2:00 AM	–4	13	–23	Partly Cloudy
3:00 AM	–4	14	–24	Fair
4:00 AM	–8	10	–26	Fair
5:00 AM	–8	15	–30	Fair
6:00 AM	–9	13	–30	Fair
7:00 AM	–13	5	–26	Fair
8:00 AM	–9	21	–34	Fair/Windy
9:00 AM	–9	16	–32	Fair
10:00 AM	–9	20	–34	Fair
11:00 AM	–8	17	–31	Drifting Snow
12:00 PM	–6	16	–28	Drifting Snow
1:00 PM	–4	21	–28	Drifting Snow/Windy
2:00 PM	0	20	–22	Drifting Snow
3:00 PM	0	21	–22	Drifting Snow/Windy
4:00 PM	1	17	–19	Drifting Snow
5:00 PM	1	12	–16	Fair
6:00 PM	0	7	–13	Fair
7:00 PM	–4	5	–15	Fair
8:00 PM	–9	3	–17	Fair
9:00 PM	–8	6	–21	Fair
10:00 PM	–8	0	n/a	Fair
11:00 PM	–9	6	–23	Fair
12:00 AM	–11	6	–25	Fair

Table A-8. Hourly weather data 22 January 2020.

Time	Temperature (°F)	Wind Speed (mph)	Wind Chill (°F)	Condition
1:00 AM	–9	8	–25	Fair
2:00 AM	–9	7	–24	Fair
3:00 AM	–9	8	–25	Fair
4:00 AM	–9	8	–25	Fair
5:00 AM	–15	6	–30	Fair
6:00 AM	–17	2	–23	Fair
7:00 AM	–15	3	–24	Fair
8:00 AM	–17	2	–23	Mostly Cloudy
9:00 AM	–15	5	–28	Mostly Cloudy
10:00 AM	–11	5	–23	Mostly Cloudy
11:00 AM	–8	3	–16	Mostly Cloudy
12:00 PM	–2	0	n/a	Mostly Cloudy
1:00 PM	–2	0	n/a	Mostly Cloudy
2:00 PM	1	6	–11	Mostly Cloudy
3:00 PM	5	3	–1	Mostly Cloudy
4:00 PM	7	0	n/a	Mostly Cloudy
5:00 PM	5	0	n/a	Fair
6:00 PM	1	3	–6	Fair
7:00 PM	–2	2	–6	Fair
8:00 PM	0	2	–4	Fair
9:00 PM	–6	0	n/a	Fair
10:00 PM	–2	7	–15	Fair
11:00 PM	5	10	–10	Fair
12:00 AM	12	10	–1	Fair

Table A-9. Hourly weather data 23 January 2020.

Time	Temperature (°F)	Wind Speed (mph)	Wind Chill (°F)	Condition
1:00 AM	12	8	0	Fair
2:00 AM	14	13	0	Mostly Cloudy
3:00 AM	16	10	4	Light Snow
4:00 AM	16	8	5	Cloudy
5:00 AM	18	6	10	Cloudy
6:00 AM	19	15	5	Light Snow
7:00 AM	18	16	3	Light Snow
8:00 AM	19	12	6	Mostly Cloudy
9:00 AM	21	14	8	Mostly Cloudy
10:00 AM	21	18	6	Light Snow Shower
11:00 AM	21	2	19	Light Snow Shower
12:00 PM	23	7	15	Cloudy
1:00 PM	25	6	18	Mostly Cloudy
2:00 PM	27	9	18	Cloudy
3:00 PM	27	13	16	Cloudy
4:00 PM	28	10	19	Cloudy
5:00 PM	28	13	17	Cloudy
6:00 PM	28	15	16	Cloudy
7:00 PM	28	17	16	Cloudy
8:00 PM	28	13	17	Cloudy
9:00 PM	27	20	13	Drifting Snow
10:00 PM	25	20	11	Cloudy
11:00 PM	23	12	11	Cloudy
12:00 AM	21	12	9	Cloudy

Table A-10. Hourly weather data 24 January 2020.

Time	Temperature (°F)	Wind Speed (mph)	Wind Chill (°F)	Condition
1:00 AM	21	10	10	Mostly Cloudy
2:00 AM	18	13	5	Light Snow Shower
3:00 AM	16	15	1	Light Snow Shower
4:00 AM	10	15	–7	Fair
5:00 AM	10	23	–10	Drifting Snow/Windy
6:00 AM	7	13	–9	Fair
7:00 AM	3	16	–16	Fair
8:00 AM	1	8	–13	Fair
9:00 AM	0	7	–13	Fair
10:00 AM	–2	16	–23	Fair
11:00 AM	–2	15	–22	Drifting Snow
12:00 PM	0	20	–22	Drifting Snow
1:00 PM	1	22	–22	Drifting Snow/Windy
2:00 PM	1	20	–21	Drifting Snow
3:00 PM	3	15	–16	Fair
4:00 PM	3	21	–18	Drifting Snow/Windy
5:00 PM	1	16	–19	Drifting Snow
6:00 PM	1	15	–18	Cloudy
7:00 PM	1	15	–18	Cloudy
8:00 PM	1	17	–19	Cloudy
9:00 PM	1	13	–17	Mostly Cloudy
10:00 PM	–2	12	–20	Fair
11:00 PM	–2	8	–17	Fair
12:00 AM	–4	5	–15	Fair

Table A-11. Hourly weather data 25 January 2020.

Time	Temperature (°F)	Wind Speed (mph)	Wind Chill (°F)	Condition
1:00 AM	–2	9	–18	Cloudy
2:00 AM	1	3	–6	Cloudy
3:00 AM	3	17	–17	Cloudy
4:00 AM	5	2	1	Cloudy
5:00 AM	5	0	39	Cloudy
6:00 AM	10	15	–7	Cloudy
7:00 AM	10	3	4	Cloudy
8:00 AM	10	9	–3	Cloudy
9:00 AM	10	12	–5	Cloudy
10:00 AM	12	9	0	Cloudy
11:00 AM	12	15	–4	Cloudy
12:00 PM	12	12	–2	Mostly Cloudy
1:00 PM	14	9	2	Mostly Cloudy
2:00 PM	14	12	0	Mostly Cloudy
3:00 PM	16	13	2	Mostly Cloudy
4:00 PM	16	7	6	Mostly Cloudy
5:00 PM	18	14	4	Mostly Cloudy
6:00 PM	16	12	3	Mostly Cloudy
7:00 PM	16	8	5	Mostly Cloudy
8:00 PM	16	8	5	Mostly Cloudy
9:00 PM	18	8	8	Mostly Cloudy
10:00 PM	14	7	4	Mostly Cloudy
11:00 PM	18	12	5	Mostly Cloudy
12:00 AM	18	16	3	Mostly Cloudy

Table A-12. Hourly weather data 26 January 2020.

Time	Temperature (°F)	Wind Speed (mph)	Wind Chill (°F)	Condition
1:00 AM	18	18	2	Partly Cloudy
2:00 AM	18	17	3	Mostly Cloudy
3:00 AM	18	17	3	Mostly Cloudy
4:00 AM	18	15	4	Cloudy
5:00 AM	18	15	4	Cloudy
6:00 AM	16	3	11	Cloudy
7:00 AM	16	0	46	Cloudy
8:00 AM	16	5	8	Mostly Cloudy
9:00 AM	14	2	11	Mostly Cloudy
10:00 AM	16	6	7	Mostly Cloudy
11:00 AM	18	7	9	Mostly Cloudy
12:00 PM	19	5	12	Mostly Cloudy
1:00 PM	21	5	14	Mostly Cloudy
2:00 PM	23	2	21	Mostly Cloudy
3:00 PM	25	0	51	Mostly Cloudy
4:00 PM	23	0	50	Mostly Cloudy
5:00 PM	21	6	13	Light Snow
6:00 PM	19	8	9	Light Snow
7:00 PM	18	6	10	Cloudy
8:00 PM	18	7	9	Light Snow
9:00 PM	16	6	7	Light Snow
10:00 PM	16	5	8	Light Snow
11:00 PM	16	5	8	Light Snow
12:00 AM	16	12	3	Light Snow

Table A-13. Hourly weather data 27 January 2020.

Time	Temperature (°F)	Wind Speed (mph)	Wind Chill (°F)	Condition
1:00 AM	14	9	2	Light Snow
2:00 AM	14	9	2	Light Snow
3:00 AM	14	16	–2	Light Snow
4:00 AM	12	15	–4	Cloudy
5:00 AM	12	18	–5	Light Snow Shower
6:00 AM	12	24	–8	Light Snow Shower/Windy
7:00 AM	12	20	–6	Light Snow Shower
8:00 AM	10	17	–8	Drifting Snow
9:00 AM	10	22	–10	Light Snow Shower/Windy
10:00 AM	10	16	–7	Light Snow Shower
11:00 AM	10	13	–5	Light Snow Shower
12:00 PM	10	13	–5	Light Snow Shower
1:00 PM	10	9	–3	Mostly Cloudy
2:00 PM	10	9	–3	Cloudy
3:00 PM	10	8	–2	Cloudy
4:00 PM	12	6	2	Cloudy
5:00 PM	10	9	–3	Cloudy
6:00 PM	10	7	–1	Cloudy
7:00 PM	9	9	–4	Cloudy
8:00 PM	9	8	–3	Cloudy
9:00 PM	7	6	–4	Cloudy
10:00 PM	7	9	–6	Cloudy
11:00 PM	7	9	–6	Cloudy
12:00 AM	5	7	–7	Cloudy

Table A-14. Hourly weather data 28 January 2020.

Time	Temperature (°F)	Wind Speed (mph)	Wind Chill (°F)	Condition
1:00 AM	5	5	–5	Cloudy
2:00 AM	5	7	–7	Cloudy
3:00 AM	5	3	–1	Cloudy
4:00 AM	5	3	–1	Cloudy
5:00 AM	5	6	–6	Cloudy
6:00 AM	5	2	1	Cloudy
7:00 AM	3	0	38	Cloudy
8:00 AM	3	3	–3	Cloudy
9:00 AM	1	8	–13	Cloudy
10:00 AM	1	9	–14	Light Snow
11:00 AM	1	6	–11	Mostly Cloudy
12:00 PM	3	8	–10	Mostly Cloudy
1:00 PM	3	9	–11	Mostly Cloudy
2:00 PM	5	13	–12	Mostly Cloudy
3:00 PM	7	17	–11	Fair
4:00 PM	7	16	–11	Fair
5:00 PM	5	16	–14	Fair
6:00 PM	3	8	–10	Fair
7:00 PM	1	9	–14	Fair
8:00 PM	0	8	–14	Fair
9:00 PM	0	9	–15	Fair
10:00 PM	1	14	–18	Mostly Cloudy
11:00 PM	1	14	–18	Mostly Cloudy
12:00 AM	1	8	–13	Cloudy

Table A-15. Hourly weather data 29 January 2020.

Time	Temperature (°F)	Wind Speed (mph)	Wind Chill (°F)	Condition
1:00 AM	1	7	–12	Light Snow Shower
2:00 AM	1	6	–11	Light Snow Shower
3:00 AM	1	7	–12	Light Snow Shower
4:00 AM	1	8	–13	Light Snow
5:00 AM	3	8	–10	Light Snow
6:00 AM	3	8	–10	Light Snow
7:00 AM	3	9	–11	Light Snow
8:00 AM	3	8	–10	Light Snow
9:00 AM	3	8	–10	Light Snow
10:00 AM	3	12	–14	Light Snow
11:00 AM	5	8	–8	Light Snow
12:00 PM	7	5	–2	Light Snow
1:00 PM	9	3	3	Light Snow
2:00 PM	10	3	4	Light Snow
3:00 PM	12	16	–5	Light Snow
4:00 PM	12	14	–4	Light Snow
5:00 PM	12	10	–1	Light Snow
6:00 PM	12	8	0	Light Snow
7:00 PM	10	6	0	Light Snow
8:00 PM	10	3	4	Light Snow
9:00 PM	10	3	4	Light Snow
10:00 PM	9	18	–9	Light Snow Shower
11:00 PM	5	15	–13	Mostly Cloudy
12:00 AM	3	14	–15	Partly Cloudy

Table A-16. Hourly weather data 30 January 2020.

Time	Temperature (°F)	Wind Speed (mph)	Wind Chill (°F)	Condition
1:00 AM	1	12	–16	Partly Cloudy
2:00 AM	–2	7	–15	Fair
3:00 AM	–4	10	–21	Fair
4:00 AM	–6	13	–26	Fair
5:00 AM	–6	10	–23	Fair
6:00 AM	–8	10	–26	Fair
7:00 AM	–8	12	–28	Fair
8:00 AM	–9	10	–27	Fair
9:00 AM	–9	5	–21	Fair
10:00 AM	–2	10	–18	Partly Cloudy
11:00 AM	0	10	–16	Partly Cloudy
12:00 PM	3	20	–18	Drifting Snow
1:00 PM	7	20	–13	Drifting Snow
2:00 PM	9	18	–9	Drifting Snow
3:00 PM	10	21	–9	Fair/Windy
4:00 PM	12	21	–7	Partly Cloudy/Windy
5:00 PM	12	22	–7	Drifting Snow/Windy
6:00 PM	12	24	–8	Drifting Snow/Windy
7:00 PM	14	16	–2	Drifting Snow
8:00 PM	14	17	–2	Cloudy
9:00 PM	14	23	–5	Drifting Snow/Windy
10:00 PM	14	14	–1	Cloudy
11:00 PM	14	14	–1	Cloudy
12:00 AM	16	14	2	Cloudy

Table A-17. Hourly weather data 31 January 2020.

Time	Temperature (°F)	Wind Speed (mph)	Wind Chill (°F)	Condition
1:00 AM	14	9	2	Light Snow Shower
2:00 AM	14	12	0	Mostly Cloudy
3:00 AM	12	13	–3	Mostly Cloudy
4:00 AM	10	6	0	Light Snow Shower
5:00 AM	10	7	–1	Cloudy
6:00 AM	12	10	–1	Mostly Cloudy
7:00 AM	12	12	–2	Mostly Cloudy
8:00 AM	12	14	–4	Mostly Cloudy
9:00 AM	14	12	0	Mostly Cloudy
10:00 AM	14	12	0	Light Snow Shower
11:00 AM	16	12	3	Light Snow Shower
12:00 PM	16	20	–1	Light Snow Shower
1:00 PM	18	21	1	Drifting Snow/Windy
2:00 PM	18	18	2	Drifting Snow
3:00 PM	19	16	4	Drifting Snow
4:00 PM	18	15	4	Drifting Snow
5:00 PM	18	21	1	Drifting Snow/Windy
6:00 PM	18	16	3	Drifting Snow
7:00 PM	16	14	2	Mostly Cloudy
8:00 PM	14	9	2	Mostly Cloudy
9:00 PM	12	7	1	Mostly Cloudy
10:00 PM	12	2	9	Mostly Cloudy
11:00 PM	14	0	n/a	Mostly Cloudy
12:00 AM	14	12	0	Mostly Cloudy

Table A-18. Hourly weather data 1 February 2020.

Time	Temperature (°F)	Wind Speed (mph)	Wind Chill (°F)	Condition
1:00 AM	10	9	–3	Fair
2:00 AM	7	8	–6	Fair
3:00 AM	7	9	–6	Fair
4:00 AM	5	14	–12	Fair
5:00 AM	5	9	–9	Fair
6:00 AM	3	8	–10	Fair
7:00 AM	1	10	–15	Mostly Cloudy
8:00 AM	3	6	–8	Cloudy
9:00 AM	3	7	–9	Cloudy
10:00 AM	5	6	–6	Mostly Cloudy
11:00 AM	9	10	–5	Mostly Cloudy
12:00 PM	12	18	–5	Mostly Cloudy
1:00 PM	14	20	–4	Partly Cloudy
2:00 PM	18	16	3	Mostly Cloudy
3:00 PM	19	18	4	Mostly Cloudy
4:00 PM	21	18	6	Cloudy
5:00 PM	19	12	6	Cloudy
6:00 PM	18	7	9	Cloudy
7:00 PM	14	3	9	Cloudy
8:00 PM	12	3	7	Partly Cloudy
9:00 PM	10	3	4	Mostly Cloudy
10:00 PM	9	3	3	Partly Cloudy
11:00 PM	5	2	1	Mostly Cloudy
12:00 AM	9	5	0	Mostly Cloudy

Table A-19. Hourly weather data 2 February 2020.

Time	Temperature (°F)	Wind Speed (mph)	Wind Chill (°F)	Condition
1:00 AM	9	5	0	Mostly Cloudy
2:00 AM	7	5	–2	Mostly Cloudy
3:00 AM	9	6	–1	Mostly Cloudy
4:00 AM	5	6	–6	Fair
5:00 AM	7	7	–5	Fair
6:00 AM	3	3	–3	Fair
7:00 AM	1	7	–12	Fair
8:00 AM	0	6	–12	Fair
9:00 AM	–2	8	–17	Fair
10:00 AM	1	6	–11	Fair
11:00 AM	5	2	1	Fair
12:00 PM	12	0	n/a	Fair
1:00 PM	12	5	4	Fair
2:00 PM	12	3	7	Fair
3:00 PM	14	5	6	Fair
4:00 PM	14	7	4	Fair
5:00 PM	10	5	1	Mostly Cloudy
6:00 PM	9	0	n/a	Mostly Cloudy
7:00 PM	5	3	–1	Mostly Cloudy
8:00 PM	5	2	1	Mostly Cloudy
9:00 PM	1	6	–11	Cloudy
10:00 PM	3	6	–8	Cloudy
11:00 PM	3	3	–3	Cloudy
12:00 AM	9	5	0	Light Snow

Table A-20. Hourly weather data 3 February 2020.

Time	Temperature (°F)	Wind Speed (mph)	Wind Chill (°F)	Condition
1:00 AM	12	6	2	Light Snow
2:00 AM	14	14	–1	Light Snow
3:00 AM	12	18	–5	Light Snow
4:00 AM	10	21	–9	Light Snow/Windy
5:00 AM	10	21	–9	Light Snow/Windy
6:00 AM	10	20	–9	Light Snow
7:00 AM	12	14	–4	Light Snow
8:00 AM	14	22	–4	Light Snow/Windy
9:00 AM	16	17	0	Light Snow
10:00 AM	18	20	2	Light Snow
11:00 AM	19	22	2	Light Snow/Windy
12:00 PM	18	18	2	Light Snow
1:00 PM	19	18	4	Light Snow
2:00 PM	21	23	5	Light Snow/Windy
3:00 PM	21	18	6	Light Snow
4:00 PM	23	20	8	Light Snow Shower
5:00 PM	25	24	10	Drifting Snow/Windy
6:00 PM	25	22	10	Drifting Snow/Windy
7:00 PM	25	25	9	Drifting Snow/Windy
8:00 PM	25	24	10	Drifting Snow/Windy
9:00 PM	25	20	11	Drifting Snow
10:00 PM	25	24	10	Light Snow Shower/Windy
11:00 PM	25	22	10	Light Snow Shower/Windy
12:00 AM	25	20	11	Drifting Snow

Table A-21. Hourly weather data 4 February 2020.

Time	Temperature (°F)	Wind Speed (mph)	Wind Chill (°F)	Condition
1:00 AM	23	21	8	Light Snow Shower/Windy
2:00 AM	23	22	8	Drifting Snow/Windy
3:00 AM	23	24	7	Drifting Snow/Windy
4:00 AM	23	21	8	Drifting Snow/Windy
5:00 AM	23	22	8	Drifting Snow/Windy
6:00 AM	21	23	5	Drifting Snow/Windy
7:00 AM	21	21	5	Drifting Snow/Windy
8:00 AM	19	23	2	Drifting Snow/Windy
9:00 AM	19	22	2	Drifting Snow/Windy
10:00 AM	16	18	0	Drifting Snow
11:00 AM	18	23	1	Drifting Snow/Windy
12:00 PM	18	21	1	Drifting Snow/Windy
1:00 PM	21	20	6	Drifting Snow
2:00 PM	23	14	11	Fair
3:00 PM	23	24	7	Drifting Snow/Windy
4:00 PM	23	21	8	Drifting Snow/Windy
5:00 PM	21	18	6	Fair
6:00 PM	21	13	8	Partly Cloudy
7:00 PM	19	12	6	Mostly Cloudy
8:00 PM	18	5	11	Mostly Cloudy
9:00 PM	19	7	10	Mostly Cloudy
10:00 PM	19	6	11	Light Snow Shower
11:00 PM	18	0	n/a	Light Snow Shower
12:00 AM	19	16	4	Light Snow Shower

Table A-22. Hourly weather data 5 February 2020.

Time	Temperature (°F)	Wind Speed (mph)	Wind Chill (°F)	Condition
1:00 AM	21	21	5	Mostly Cloudy/Windy
2:00 AM	19	14	5	Mostly Cloudy
3:00 AM	18	13	5	Mostly Cloudy
4:00 AM	16	15	1	Mostly Cloudy
5:00 AM	14	8	3	Mostly Cloudy
6:00 AM	12	16	–5	Fair
7:00 AM	12	15	–4	Cloudy
8:00 AM	12	9	0	Cloudy
9:00 AM	12	17	–5	Cloudy
10:00 AM	12	22	–7	Drifting Snow/Windy
11:00 AM	12	25	–8	Drifting Snow/Windy
12:00 PM	12	20	–6	Light Snow Shower
1:00 PM	12	22	–7	Light Snow Shower/Windy
2:00 PM	10	21	–9	Drifting Snow/Windy
3:00 PM	10	20	–9	Drifting Snow
4:00 PM	10	25	–11	Drifting Snow/Windy
5:00 PM	9	24	–12	Drifting Snow/Windy
6:00 PM	7	28	–16	Drifting Snow/Windy
7:00 PM	5	22	–16	Drifting Snow/Windy
8:00 PM	5	25	–17	Drifting Snow/Windy
9:00 PM	3	25	–20	Drifting Snow/Windy
10:00 PM	3	26	–20	Drifting Snow/Windy
11:00 PM	1	30	–25	Drifting Snow/Windy
12:00 AM	1	24	–22	Drifting Snow/Windy

Appendix B: Detailed Compacted Snow Placement Procedure for Various Snow Moisture Conditions

B.1 Patching Procedure Using *Ideally Moist* Snow.

1. Identify an adequate source of clean snow and prepare it for use as patch material by disaggregating clumping due to existing ice particle bonds. This can be achieved by processing through a snowblower, tumbling the snow along a hard surface with a snowplow, or dropping from the loader bucket onto a hard surface.

2. Move the harvested snow to the perimeter of the prepared crater, placing the snow in windrows on at least two sides in a quantity equal to that necessary for the first lift of the crater patch (see Table B-1 for guidance on lift thicknesses). The volume of borrow snow required will be approximately 1.5 times the volume of the finished lift (due to compaction). Windrows should be approximately 3 ft fully displaced from the edge of the prepared crater (Figure B-1).

Figure B-1. Snow placed beside repair in preparation for processing and placement.

3. Operate the snowblower along the windrow, parallel to the edge of the crater, directing ejected snow into the crater in as uniform a layer as possible (Figure B-2).

Figure B-2. Snow being blown into crater in lifts in preparation for leveling and compaction.

Table B-1. Target for lift thickness when patching craters with ideally moist snow.

Lift	Placed Thickness (in.)	Compacted Thickness (in.)
Base (First Lift)	10	7
Second through Penultimate	7	5
Top	6	4

4. Manually distribute the snow to a uniform thickness with a level surface throughout the cavity immediately after placement by the snowblower (Figure B-3). Ensure that the snow is firmly in contact with all vertical edges of the crater, especially in each corner.

Figure B-3. Manual leveling of snow blown into crater.

5. Compact the snow immediately after leveling. This is most efficiently achieved with a vibratory plate compactor (Figure B-4) but can also be effective using a "jumping jack," especially in the crater corners (Figure B-4). Tamping using a bearing plate or a curled bucket on an excavator or backhoe can also be used, but this is not as efficient or effective. Compaction activities should traverse the entire top of the snow lift with three passes. However, if the snow is being displaced rather than consolidated, the compaction effort must immediately be stopped. Either a lessor compaction effort must be applied, or the snow lift must be left as is to sinter for several hours before the next lift is placed.

Figure B-4. Vibratory plate compactor consolidating the top of a completed lift.

6. Borrow snow for the next lift should be delivered to the crater edges (see step 2 above) while leveling and compaction of the lift is being accomplished.

7. Construct each subsequent lift of the crater patch by repeating steps 3 through 6.

8. The final lift, representing the top of the crater patch, must be approximately two inches above the surrounding (undamaged) pavement.

9. Final compaction is achieved with a moderate-sized vibratory drum roller (10,000–15,000 lb operating weight; Figure B-5) when the finished patch

has been allowed to set up adequately. Set up time before final compaction is temperature dependent, with 1 hr being adequate below –4°F, but up to 3 hr when temperatures approach 30°F.

Figure B-5. Vibratory drum roller compacting top of a completed crater patch.

B.2 Patching Procedure Using Snow That is *Too Dry*.

Airfield damage repair with snow that is too dry follows the same process described in Section B.1 with the addition of activities in both steps 1 and 2 as follows:

1. Locate a source of fresh water and select a means to deliver the water to the repair site. Cool the water to a low temperature, ideally less than 50°F, but not more than 60°F prior to its arrival at the repair site. The water volume required is 33 gal./yd^3 of snow.

2. The snow must be wetted with the cold water once placed in windrows and just prior to being blown into the repair. It is important to distribute the water over the windrowed snow as uniformly as possible. This can be done with a hose (ideally at least 2 in. in diameter), or directly from a moving spigot on a mobile tank. Obviously, working with water in a cold environment imposes challenges and risks to both personnel and equipment. Effective mixing of the water with the snow will be achieved in step 3 with the snowblower.

B.3 Patching Procedure Using Snow That is *Too Wet*.

Airfield damage repair can still be achieved when only overly moist (wet) snow is available, but it is more challenging. In the best-case scenario, existing frozen ground and a forecast of well below freezing air temperatures for at least a week will allow wet snow to be placed into the repair. The wet snow will freeze to form an adequately dense, bonded material that can resist heavy aircraft wheel loads and tire pressures. Levels of "too wet" can be divided into two categories: wet and saturated. Airfield repairs with wet snow (yields snowball with "eggshell" surface) can conducted by following the steps outlined in section B-1 with the following addition:

1. For lift thicknesses, Table B-2 must be used in place of Table B-1. Less compaction effort will also be realized in achieving a dense snow (compacted thickness levels in Table B-2).

Table B-2. Target lift thickness when patching craters with wet snow.

Lift	Placed Thickness (in.)	Compacted Thickness (in.)
Base (First Lift)	7	6
Second through Penultimate	5	4
Top	4	3

Saturated snow is marked by water free draining (dripping) from a hand-squeezed volume of snow. Patching using saturated snow is possible, but curing times (complete freeze) can make this approach unfeasible. Typically, snow becomes saturated because of a warm, melting event or rain. A search for borrow snow in perpetually shaded and protected areas (e.g., behind the north side or under roof overhangs of a large building or within a forested area) may yield material with a notably lower water content. Similarly, snow in the interior of large piles of snow (e.g., plowed parking areas or large berms along runway or apron edges) may have been protected from the full brunt of warm temperatures or rain and thus be less wet. This may require a longer travel distance to acquire the best patching material.

Patching with saturated snow can be conducted as described in Section B.1 with the following exceptions:

- Saturated snow's ice particles will not be bonded, meaning disaggregation is not necessary.

- Saturated snow can be placed in the cavity directly by dump truck or loader (no snowblower needed). The snow should still be placed in lifts as prescribed in Table B-2, and raked level.
- Saturated snow cannot be compacted, owing to the presence of free water in the pore spaces. Thus, steps 5 to 7 in Section B-1 can be omitted. In step 8 of Section B-1, the level of saturated snow must be flush with the surrounding undamaged runway.
- During curing, the large volume of water present in the patched area when using saturated snow is great enough that heaving (blistering) should be expected. If this occurs, shaving or screeding must be performed prior to aircraft traffic. Depending on equipment availability, this leveling can be done at intervals during curing, or it can be accomplished when curing is complete and the patch can support heavy equipment (e.g., grader) that has the capability of shaving off any icy blister.

Under similar temperature conditions (ground and air), curing time for both wet snow and saturated snow will be greater than for ideally moist snow. The more water present in the snow, the more latent heat must be removed to create ice. This phase transformation cannot be hastened except by colder boundary temperatures. Still, freezing will take place from the cold borders (primarily the top of the patch and, to a lesser degree, the vertical sides of the crater where frozen soil exists) inward to the center of the patched mass. Achieving curing of the entire patched volume can, depending on boundary conditions, take days.

B.4 Patching Procedure Using Cellulose Added to Snow.

If cellulose is to be added to snow, the procedures in this section can be used, For ideally moist snow, steps 1 and 2 in Section B-1 will include the following:

1. Prepare containers of bulk cellulose slurry (e.g., 40 gal. drums at 5% cellulose concentration) by cold soaking to a temperature ideally less than 50°F but not more than 60° prior to its arrival at the repair site. The drummed cellulose volume required is 7 gal./yd^3 of snow.

2. The snow must be topped with cellulose once placed in windrows and just prior to being blown into the repair. This can be achieved simply by scooping (with shovels or buckets) liquefied cellulose from the bulk container and spreading it as uniformly as possible along the tops of the

snow windrows. Effective mixing of the cellulose with the snow will be achieved in step 3 with the snowblower.

For too dry snow, the two added steps described previously are employed. When using dry snow for a crater patch including cellulose, further additions are as follows:

1. Prepare containers of bulk cellulose slurry (e.g., 40 gal. drums at 5% cellulose concentration) by cold soaking to a temperature ideally less than 50°F but not more than 60° prior to its arrival at the repair site. The drummed cellulose volume required is 7 gal./yd^3 of snow.

2. The snow must be topped with cellulose once placed in windrows and wetted with water, just prior to being blown into the repair. This can be achieved simply by scooping (with shovels or buckets) liquefied cellulose from the bulk container and spreading it as uniformly as possible along the tops of the snow windrows. Effective mixing of the cellulose with the water and the snow will be achieved in step 3 with the snowblower.

In the case of too wet snow, patching will follow the process described previously (using Table B-2 instead of Table B-1), again with the modifications for adding cellulose prior to placement. Thus, the following steps are added:

1. Prepare containers of bulk cellulose slurry (e.g., 40 gal. drums at 5% cellulose concentration) by cold soaking to a temperature ideally less than 50°F but not more than 60° prior to its arrival at the repair site. The drummed cellulose volume required is 7 gal./yd^3 of snow.

2. The snow must be topped with cellulose once placed in windrows and just prior to being blown into the repair. This can be achieved simply by scooping (with shovels or buckets) liquefied cellulose from the bulk container and spreading it as uniformly as possible along the tops of the snow windrow.

Abbreviations

ADR	Airfield damage repair
AFB	Air Force Base
ASTM	American Society for Testing and Materials
CARTS	Concrete Airfield Repair Thermal Simulator
CBR	California Bearing Ratio
CRATR	Critical Runway Assessment and Repair
CRREL	Cold Regions Research and Engineering Laboratory
CSA	Calcium sulfoaluminate
CTL	Compact track loaders
DCP	Dynamic cone penetrometer
ERDC	US Army Engineer Research and Development Center
FERF	Frost Effects Research Facility
FOD	Foreign object debris
FRP	Fiber-reinforced polyester
GSL	Geotechnical and Structures Laboratory
HDPE	High-density polyethylene
HWD	Heavy weight deflectometer
ISM	Impulse-stiff modulus
JCTD	Joint Capabilities Technology Demonstration
LOUA	Limited operational utility assessments
MOS	Minimum operating strip
OUA	Operational utility assessment

PCC	Portland cement concrete
RADR	Rapid Airfield Damage Recovery
RSC	Rapid-setting concrete
RSFF	Rapid-setting flowable fill
RSP	Russian Snow Penetrometer
SP	Poorly graded sand
SVM	Simplified Volumetric Mixer
T.O.	Technical Order
TTPs	Tactics, techniques, and procedures
UCS	Unconfined compressive strength
USAF	US Air Force
USCS	Unified Soil Classification System
UTC	Unit type code
VMFF	Volumetrically mixed flowable fill

REPORT DOCUMENTATION PAGE

1. REPORT DATE	2. REPORT TYPE	3. DATES COVERED	
		START DATE	END DATE
January 2024	Final Report	FY19	FY20

4. TITLE AND SUBTITLE

Extreme Cold Weather Airfield Damage Repair Testing at Goose Bay Air Base, Canada

5a. CONTRACT NUMBER	5b. GRANT NUMBER	5c. PROGRAM ELEMENT
5d. PROJECT NUMBER	**5e. TASK NUMBER**	**5f. WORK UNIT NUMBER**

6. AUTHOR(S)

William D. Carruth, Terry D. Melendy, Jr., George L. Blaisdell, Benjamin E. Watts, Danielle Kennedy, Jeb S. Tingle, and Alessandra Bianchini

7. PERFORMING ORGANIZATION NAME(S) AND ADDRESS(ES)

Geotechnical and Structures Laboratory (GSL)
US Army Engineer Research and Development Center (ERDC)
3909 Halls Ferry Road
Vicksburg, MS 39180-6199

8. PERFORMING ORGANIZATION REPORT NUMBER

ERDC TR-24-3

9. SPONSORING/MONITORING AGENCY NAME(S) AND ADDRESS(ES)	10. SPONSOR/MONITOR'S ACRONYM(S)	11. SPONSOR/MONITOR'S REPORT NUMBER(S)
US Air Force Civil Engineer Center (AFCEC) 139 Barnes Drive, Suite 1 Tyndall AFB, FL 32403 Office of the Under Secretary of Defense for Acquisition and Sustainment – International Cooperation 1400 Defense Pentagon Washington, DC 20301	AFCEC	

12. DISTRIBUTION/AVAILABILITY STATEMENT

Distribution Statement A. Approved for public release: distribution is unlimited.

13. SUPPLEMENTARY NOTES

14. ABSTRACT

Rapid Airfield Damage Recovery (RADR) technologies have proven successful in temperate and subfreezing temperatures but have not been evaluated in extreme cold weather temperatures near 0ºF. To address this capability gap, laboratory-scale and full-scale testing was conducted at these temperatures. Methods developed for moderate climates were adapted and demonstrated alongside methods that used snow harvested on-site as compacted backfill. After only a few days of training, seven experimental repairs were conducted by Canadian airmen at Goose Bay Air Base in Labrador, Canada, and load tested with a single-wheel C-17 load cart. Existing RADR technologies performed adequately despite the freezing temperatures, with the main tactic, techniques, and procedures modification being an increased cure time for the rapid-setting concrete surface material. Compacted snow-water slurry methods also performed well, demonstrating their ability to withstand over 500 passes of single-wheel C-17 traffic after sufficient freezing time.

15. SUBJECT TERMS

Airfield Damage Repair; Cold Regions; Cold Weather Effects; Compacted Snow and Ice; Concrete—Cold Weather Conditions; Fiber Reinforced Polymer Matting; Flowable Fill Backfill; Geocells; Military Bases; Rapid Runway Repair; Rapid-Setting Concrete; Runways (Aeronautics)—Maintenance and Repair

16. SECURITY CLASSIFICATION OF:			17. LIMITATION OF ABSTRACT	18. NUMBER OF PAGES
a. REPORT	b. ABSTRACT	C. THIS PAGE		
Unclassified	Unclassified	Unclassified	SAR	138

19a. NAME OF RESPONSIBLE PERSON	19b. TELEPHONE NUMBER
William D. Carruth	